HHS Public Access

Author manuscript

Mol Cell. Author manuscript; available in PMC 2019 September 20.

Published in final edited form as:

Mol Cell. 2018 September 20; 71(6): 973–985.e5. doi:10.1016/j.molcel.2018.08.011.

Differential m^{6}A, m^{6}A$_m$, and m^{1}A Demethylation Mediated by FTO in Cell Nucleus and Cytoplasm

Jiangbo Wei[#1,2], **Fange Liu**[#1,2], **Zhike Lu**[1,2,3], **Qili Fei**[1,2], **Yuxi Ai**[1,2], **P. Cody He**[1,2], **Hailing Shi**[1,2], **Xiaolong Cui**[1,2], **Rui Su**[4], **Arne Klungland**[5], **Guifang Jia**[6], **Jianjun Chen**[4], and **Chuan He**[1,2,3,*]

[1]Department of Chemistry, Department of Biochemistry and Molecular Biology, and Institute for Biophysical Dynamics, The University of Chicago, 929 East 57 Street, Chicago, Illinois 60637, USA

[2]Howard Hughes Medical Institute, The University of Chicago, 929 East 57 Street, Chicago, Chicago, Illinois 60637, USA.

[3]Institute of Natural Sciences, Westlake Institute for Advanced Study, Westlake University, 18 Shilongshan Road, Hangzhou 310064, China

[4]Department of Systems Biology, Beckman Research Institute of City of Hope, Monrovia, California 91016, USA

[5]Institute of Medical Microbiology, Oslo University Hospital, Rikshospitalet, Norway Institute of Basic Medical Sciences, University of Oslo, PO Box 1018 Blindern, N-0315 Oslo, Norway.

[6]Synthetic and Functional Biomolecules Center, Beijing National Laboratory for Molecular Sciences, Key Laboratory of Bioorganic Chemistry and Molecular Engineering of Ministry of Education, College of Chemistry and Molecular Engineering, Peking University, Beijing 100871, China

[#] These authors contributed equally to this work.

Summary

FTO, the first RNA demethylase discovered, mediates the demethylation of internal N^6-methyladenosine (m^{6}A) and N^6, 2-O-dimethyladenosine (m^{6}A$_m$) at the +1 position from the 5’

[*]Lead contact. Correspondence: chuanhe@uchicago.edu.

AUTHOR CONTRIBUTION

J.W., F. L., and C.H. conceived the project and designed experiments. J.W. and F. L. performed experiments with help from Y.A. J.W. analyzed data with help from Z.L., Q.F. and P.C.H. Z.L. and Q.F. processed the high-throughput RNA sequencing data. S.H. and X.C. assisted data analysis. A.K. established the *Fto*$^{-/-}$ MEF cell line and contributed *Fto*$^{-/-}$ and the wild-type mouse brain. R.S. and J.C. contributed AML cells and relevant studies. G.J. provided reagents. J.W., F. L., and C.H. wrote the manuscript with input from P.C.H and comments from A.K., J.C, and G.J.

SUPPLEMENTAL INFORMATION

Supplemental information including six figures and four tables can be found with this article online.

DECLARATION OF INTERESTS

Chuan He is a scientific founder of Accent Therapeutics, Inc. and a member of its scientific advisory board.

cap in mRNA. Here, we demonstrate that the cellular distribution of FTO is distinct among different cell lines, affecting the access of FTO to different RNA substrates. We find that FTO binds multiple RNA species, including mRNA, snRNA, and tRNA, and can demethylate internal m^6A and cap m^6A in mRNA, internal m^6m A in U6 RNA, internal and cap m^6A_m in snRNAs, and N^1-methyladenosine (m^1A) in tRNA. FTO-mediated demethylation shows a greater impact on the transcript levels of mRNAs possessing internal m^6A than the ones with cap m^6A_m in the tested cells. We also show that FTO can directly repress translation by catalyzing m^1A tRNA demethylation. Collectively, FTO-mediated RNA demethylation occurs to m^6A and m^6A_m in mRNA and snRNA as well as m^1A in tRNA.

In Brief

Wei et al. show that FTO mediates internal m^6A and cap m^6A_m demethylation of polyadenylated RNA with differential substrate preferences in nucleus *versus* cytoplasm, in which the internal m^6A demethylation correlates with transcript level changes. FTO also affects snRNA m^6A and m^6A_m levels and mediates tRNA m^1A demethylation.

Abstract

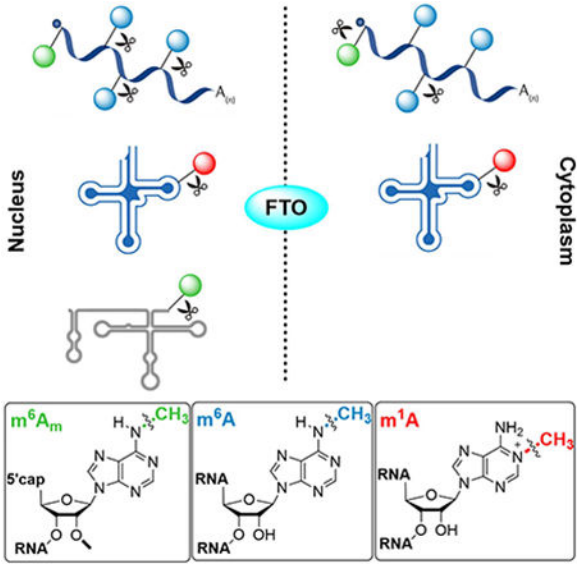

Introduction

FTO was suggested to be associated with human obesity by GWAS (Fawcett and Barroso, 2010). A genetic variant of FTO has been shown to be associated with increased food intake (Cecil et al., 2008) while loss-of-function mutations in FTO cause severe growth retardation (Boissel et al., 2009) and CNS defects (Ho et al., 2010), which were recapitulated in murine model studies (Church et al., 2010; Fischer et al., 2009; Hess et al., 2013).

Due to these intriguing phenotypes, extensive efforts have been devoted to identify the substrate(s) and to understand the biological function of FTO. FTO was first reported to catalyze the demethylation of 3-methylthymine (3meT) in single-stranded DNA (Gerken et

al., 2007) and 3-methyluracil (3meU) in RNA (Jia et al., 2008) as an iron(II)- and αKG-dependent dioxygenase. Later, FTO was identified as the first RNA demethylase that catalyzes reversal of the N^6-methyladenosine (m^6A) methylation in mRNA *in vitro* and inside cells (Fu et al., 2013; He, 2010; Jia et al., 2011). m^6A is the most abundant internal modification in mammalian mRNAs (Fu et al., 2014). Adjacent to the 5' cap, the second base in many mRNAs can be 2'-*O*-methylated (Adams and Cory, 1975; Wei et al., 1975b), with a portion of these bases also bearing m^6A methylation to form m^6A_m (Wei et al., 1975a), deposited by a yet to be identified methyltransferase. This modification was confirmed by transcriptome-wide m^6A-seq and exists in considerably lower overall abundance compared with m^6A (Linder et al., 2015; Molinie et al., 2016). The m^6A portion of m^6A_m is known to be an *in vitro* substrate of FTO (Fu, 2012), with a recent study showing that m^6A_m stabilizes mRNA by preventing DCP2-mediated decapping and microRNA-mediated mRNA degradation (Mauer et al., 2017). However, the functional relevance of m^6A_m removal by FTO has yet to be fully explored.

Surprisingly, this study also suggested that internal mRNA m^6As may not be relevant substrates of FTO (Mauer et al., 2017), despite reports of a range of biological processes affected by the demethylation of internal m^6A in the last several years: i) FTO-mediated m^6A demethylation is critical in DNA UV damage response, with the m^6A methyltransferase complex METTL3/14 exhibiting the opposite function (Xiang et al., 2017); ii) FTO plays noticeable roles in *Flaviviridae* family viruses infection *via* demethylating viral RNA m^6A in host cells (Gokhale et al., 2016); certain members such as hepatitis C virus do not possess cap nor cap m^6A_m but still respond to FTO; iii) FTO-catalyzed demethylation significantly affects glioblastoma stem cell differentiation, again with METTL3/14 showing opposing functions (Cui et al., 2017); iv) FTO mediates nuclear demethylation of m^6A at the 5' UTR in heat shock response (Zhou et al., 2015); v) internal m^6A demethylation by FTO plays an oncogenic role in a subset of acute myeloid leukemia (Li et al., 2017), and the effect of 2-HG inhibition can be explained through internal m^6A methylation changes to oncogenic transcript targets of FTO, such as MYC (Su et al., 2018); vi) using liver-specific *Fto*-transgenic mice Fto was shown to mediate both m^6A and cap m^6A_m demethylation; however, internal m^6A demethylation controls the alternative translation (Zhou et al., 2018); vii) demethylation of internal m^6A on a specific mRNA by FTO facilitates the stability and translation of the target transcript in neuronal developments (Yu et al., 2018); and viii) a recent report showing that FTO binds extensively across mRNA and intron regions in premRNA (Bartosovic et al., 2017).

In our biochemical studies, we confirmed that FTO could effectively demethylate both m^6A and cap m^6A_m from purified polyadenylated RNA. We were intrigued by how FTO demethylates m^6A and/or m^6A_m on target polyadenylated RNAs inside cells and the different functional consequences of the demethylation. We found that FTO localization within the nucleus and cytoplasm varies between cell types and that FTO has distinct substrate repertoires inside the cell nucleus and cytoplasm. We further identified additional RNA substrates of FTO, including m^1A in tRNA, m^6A in U6 RNA, internal and cap m^6A_m in snRNAs. This study presents the most comprehensive picture of the FTO-mediated RNA demethylation to date. It reveals a previously unappreciated spatial regulation imparted by

nuclear *versus* cytoplasmic demethylation mediated by FTO, which exerts distinct effects on target RNAs.

Results

FTO Mediates Demethylation of Both m^6A and m^6A_m *in vitro* and inside Cells

FTO has been shown to demethylate both m^6A and m^6A_m (Fu, 2012; Fu et al., 2013; Jia et al., 2011; Mauer et al., 2017) (Figure 1A). To further validate these previous reports with biologically relevant substrates, we isolated polyadenylated RNAs possessing both naturally occurring m^6A and m^6A_m from HEK293T cells and performed *in vitro* demethylation using purified FTO (Figure S1A). The substrate polyadenylated RNAs were digested to single nucleosides after FTO treatment. Ultra-High-performance liquid chromatography-tandem mass spectrometry **(**UHPLC-MS/MS) was utilized to quantify levels of both m^6A and m^6A_m from digested RNAs using carefully calibrated standard curves generated using synthetic nucleoside standards (Figure S1B).

As shown in Figure S1C, among HeLa, HEK293T, and 3T3-L1 cells, the levels of m^6A_m in polyadenylated RNAs are about 1/10 to 1/15 of that of m^6A. FTO (2 μM in 20 ul) is capable of almost complete demethylation of all m^6A_m and 81.4% of m^6A in 200 ng polyadenylated RNAs within 1 hour under reported demethylation conditions (Figure S1D) (Jia et al., 2011; Mauer et al., 2017). The use of EDTA in the same reaction, which chelates the essential iron cofactor, serves as a control. We further lowered the FTO concentration to achieve incomplete demethylation of cap m^6A_m in isolated polyadenylated RNAs and compared the global changes of m^6A and m^6A_m. As shown in Figure S1E, 0.2 μM of FTO (20 ul) could demethylate 81.9% of m^6A and 20.3% m^6 m A in the purified polyadenylated RNAs. Our results unequivocally show that FTO demethylates both internal m^6A and cap m^6A_m in purified polyadenylated RNAs *in vitro*. FTO exhibits higher activity towards m^6A_m; however, it should be noted that because the total amount of m^6A is around 10-fold to 15-fold higher than that of m^6A_m in polyadenylated RNAs (Figure S1C), more m^6As are demethylated compared to m^6A_m in purified polyadenylated RNAs in terms of the number of modifications that can be reversed by FTO *in vitro*.

Next, we evaluated the effects of FTO perturbation on the cellular m^6A and m^6A_m levels of polyadenylated RNAs. We selected HeLa, HEK293T, and 3T3-L1 cell lines and measured the levels of m^6A and m^6A_m upon transient knockdown of FTO in comparison to the knockdown control by using UHPLC-MS/MS. A 19.2%, 11.8%, and 8.8% increase of the m^6A/A ratio was observed in the polyadenylated RNAs in the knockdown samples compared to the knockdown control in HeLa, HEK293T, and 3T3-L1 cell lines, respectively (Figure 1B, blue bars). For m^6A_m, a 13.7%, 20.6%, and 30.1% increase was consistently observed in the FTO knockdown samples compared to the knockdown control in HeLa, HEK293T, and 3T3-L1 cells, respectively (Figure 1B, green bars). The knockdown efficiency was validated by western blots (Figure S1F). These results revealed that the demethylation percentage of m^6A inside cells by FTO is more profound in HeLa cells in comparison to HEK293T and 3T3-L1, while the FTO-mediated demethylation of m^6A_m is more evident in 3T3-L1 cells compared to the other two cell lines. It again demonstrated both m^6A and m^6A_m demethylation by FTO inside different cell lines. Because the level of

internal m^6A is 10-fold higher than that of cap m^6A_m in these cells, 5–10 times more internal m^6A are subjected to FTO-mediated demethylation compared with m^6A_m inside cells.

FTO Preferentially Targets Nuclear m^6A and Both Cytoplasmic m^6A and m^6 m A in mRNA

We sought to investigate how FTO mediates differential m^6A *versus* m^6A_m demethylation in different cell lines and why FTO exhibits much higher m^6A demethylation (over ~10-fold) *versus* m^6A_m inside certain cells such as HeLa despite m^6A_m being a preferred *in vitro* substrate. We reasoned that as almost all mRNA caps are bound by cap-binding proteins inside the cell nucleus (Muller-McNicoll and Neugebauer, 2013), the lack of m^6A_m demethylation in certain cells might reflect substrate accessibility by FTO. FTO was first reported to be a nuclear protein, but it was later shown to exist in both cell nucleus and cytoplasm in different mammalian cell lines (Aas et al., 2017; Gulati et al., 2014). We asked whether the spatial regulation of FTO plays a crucial role in gaining access to its physiologically relevant substrate(s). We conducted confocal immunofluorescence (IF) imaging with an anti-FTO specific antibody to investigate the cellular localization of FTO in five mammalian cell lines: HeLa, Mel624, HepG2, HEK293T, and 3T3-L1 cell lines. As shown in Figure 2A, the relative proportion of FTO within the nucleus and cytoplasm varies across cell lines. In HeLa, Mel624, and HepG2 cells, FTO predominantly accumulates in the cell nucleus. However, FTO is located in both cell nucleus and cytoplasm in HEK293T cells. The presence of FTO in the cytoplasm is even more notable in 3T3-L1 cells than HEK293T cells. More immunofluorescent images for HeLa, HEK293T, and 3T3-L1 were collected and five representative pictures from each cell line were shown in the Figure S2A. Calculated by ImageJ, the colocalization of the endogenous FTO with the nucleus was 97.7%, 83.5%, and 61.8% in HeLa, HEK293T, and 3T3-L1 cells, respectively. Consistent with our hypothesis, the increasing proportions of cytoplasmic FTO from HeLa, HEK293T, to 3T3-L1 cells, correlate with the corresponding increased cellular demethylation percentage towards m^6A_m and reduced m^6A demethylation percentage in these cell lines (Figure 1B).

We next expressed an FTO mutant lacking the nuclear localization signal (ΔNLS-FTO) (Aas et al., 2017; Sanchez-Pulido and Andrade-Navarro, 2007) in HEK293T cell lines. The LCMS/MS results showed that overexpression of ΔNLS-FTO, which is directed to the cytoplasm, decreases m^6A_m but not m^6A in polyadenylated RNA HEK293T cells. This result contrasts with the effects caused by wild-type FTO overexpression mostly within nucleus (Figure S2B). Next, we separated the cell nuclear and cytoplasmic fractions in HEK293T cells and then measured FTO-mediated demethylation of m^6A and m^6A_m in polyadenylated RNAs in each fraction. As shown in Figure 2B (blue bars) knockdown of FTO led to a 37.9% increase in the m^6A level in the cell nucleus but only a slight increase in the m^6A level in cytoplasmic polyadenylated RNAs. In contrast, m^6A_m in cytoplasmic but not nuclear polyadenylated RNAs is significantly increased upon FTO knockdown (Figure 2B, green bars). Furthermore, in HEK293T cells, overexpression of wild-type FTO but not ΔNLS-FTO led to a significant decrease of m^6A in polyadenylated RNAs in the cell nucleus, while the nuclear m^6A_m level in polyadenylated RNAs was not notably affected (Figure S2C). In the cytoplasm, m^6A in polyadenylated RNA showed a small percentage change upon FTO overexpression, but m^6A_m showed a larger decrease upon overexpression of

ΔNLS-FTO than wild-type FTO (Figure S2D). The separation of nucleus and cytoplasm for HEK293T cells was validated by western blot (Figure S2E) and qRT-PCR (Figure S2F). The result further confirmed that the FTO-mediated demethylation of m^6A is prominent in the cell nucleus, whereas cap m^6A_m is more a target of FTO in the cytoplasm.

Because the m^6A level is at least 10-fold higher than that of cap m^6A_m in mRNA, even in the cytoplasm FTO still mediates effective m^6A and cap m^6A_m demethylation, in absolute terms. In certain AML cell lines in which we showed proliferation inhibition with FTO knockdown previously (Li et al., 2017), stable knockdown of FTO led to increased m^6A in both nucleus and cytoplasm, whereas m^6A_m only increased in the cytoplasmic but not nuclear fraction (Figure 2C, and Figure S2G-S2J). We found extensive cytoplasmic expression of FTO in these AML cell lines (Figure S2K), and quite dramatic cytoplasmic m^6A demethylation (around 40% increase of the m^6A level with FTO knockdown), suggesting the critical cytoplasmic m^6A demethylation roles of FTO in these cells. It is noteworthy that unlike the ratio of 1/10 to 1/15 between m^6A_m and m^6A in HeLa, HEK293T, and 3T3-L1 cells (Figure S1C), the m^6A_m to m^6A ratio is among 1/25 to 1/30 in the NB4, MONOMAC-6 cells (Figure 2C), and several other AML cells (Li et al., 2017; Su et al., 2018).

FTO-mediated m^6A Demethylation in mRNA Influences Transcript Level of Target mRNA

To understand the functional impact of m^6A *versus* m^6A_m demethylation by FTO in mRNA, we analyzed transcript level changes of m^6A and m^6A_m-containing transcripts upon FTO knockdown in HEK293T cells. The m^6A sites were adopted from a previously published meRIP sequencing database (Meyer et al., 2012), and the transcripts starting with m^6A_m were obtained from the previously published study (Mauer et al., 2017). Almost all of these annotated m^6A_m sites are found within 500 nt from the transcription start site (TSS) (Figure S3A, top panel). To determine the individual effects of cap m^6A_m and internal m^6A and to avoid cross-effects between these two modifications, we classified transcripts into four groups. The first group of transcripts contains only m^6A_m but not m^6A, the second group of transcripts contains only m^6A but not m^6A_m, the third group of transcripts contains both modifications, and the rest of transcripts were considered as the fourth control group to compare against (Figure S3A bottom panel and Table S1). As shown in Figure 3A, using this classification scheme, we found that the global levels of transcripts containing only m^6A_m don't appear to statistically change upon FTO knockdown in HEK293T cells, while the global transcript levels of the other three groups show statistically noticeable increases.

Transient knockdown of FTO led to increased transcript levels of the transcripts harboring only m^6A compared to the transcripts without m^6A or m^6A_m in HEK293T cells (Figure 3B). It has previously been observed that increased m^6A leads to increased mRNA transcript levels in HepG2 and leukemia cell lines (Huang et al., 2017a; Li et al., 2017). This effect was thought to be mediated by a group of newly identified m^6A reader proteins IGF2BP1–3 (Huang et al., 2017a), which bind internal m^6A and stabilize methylated mRNAs, or through other yet to be discovered reading mechanisms.

The presence of m^6A_m adjacent to the 5' cap was previously reported to stabilize mRNA transcripts by preventing DCP2-mediated cap cleavage and microRNA-mediated mRNA

degradation in HEK293T cells (Mauer et al., 2017). However, compared to the other three groups of transcripts (Figure 3B), transcripts containing only m^6A_m but not m^6A showed significantly lower transcript level changes upon FTO knockdown. FTO knockdown should lead to elevated m^6A_m but this does not appear to correlate with higher levels of these transcripts, despite the proposed transcript-stabilizing role of m^6A_m at the cap (Mauer et al., 2017). This effect is opposite from those observed for transcripts containing both m^6A_m and m^6A or transcripts containing only m^6A. Both of the latter two groups showed significantly larger increases in transcript levels upon FTO knockdown in comparison to the control group. Lastly, grouping just transcripts containing m^6A *versus* non-m^6A without considering m^6A_m, and transcripts containing cap m^6A_m *versus* non-m^6A_m without considering m^6A, transcripts containing m^6A showed increased transcript levels upon FTO knockdown (Figure S3B), while transcripts containing m^6A_m showed reduced levels compared with the rest upon FTO knockdown (Figure S3C).

These results suggest that though m^6A_m could be associated with a higher global transcript level and higher transcript stability, the levels of transcripts bearing cap m^6A_m dos not appear to change with the knockdown of FTO (Figure 3A). The level change of these transcripts was significantly less than the transcripts containing neither m^6A_m nor m^6A upon FTO knockdown, whereas transcripts containing m^6A or both m^6A and m^6A_m had significantly larger increases in their transcript levels than transcripts containing neither or just cap m^6A_m upon FTO knockdown (Figure 3B). We further cross-compared the list of transcripts contain only m^6A but not m^6A_m with the published FTO CLIP-seq results (Bartosovic et al., 2017) by separating transcripts contains only m^6A but not m^6A_m plus FTO binding into FTO targets and non-targets. Compared to the rest genes (genes except transcripts containing only m^6A), we clearly observed in Figure 3C a statistically significant right-shift of the cumulative curve representing the increased transcript levels of the m^6A targets (bound by FTO), with no significant change for non-targets possessing m^6A but not bound by FTO. qRT-PCR was used to validate the relative transcript levels of three genes containing only m^6A or m^6A_m. The transcript level changes of these genes upon FTO knockdown were consistent with the RNA-seq data (Figure S3D).

FTO Demethylates m^6A in U6 RNA and m^6A_m in snRNAs

Two recent studies have surveyed FTO-bound RNA species through eCLIP-seq (Van Nostrand et al., 2016) or CLIP-seq of FLAG-tagged FTO (Bartosovic et al., 2017). These studies and our CLIP-seq results in 3T3-L1 cells using FLAG-tagged FTO showed that FTO is able to bind mRNA, tRNA, snRNA, snoRNA (Figure 4A, bar), and rRNA, among which mRNA is enriched (Figure 4A, donut). The purity of anti-FLAG-tagged pulldown was validated in Figure S4A (left) in our studies, and the ^{32}P labeled protein gel of CLIP is shown in Figure S4A (right), showing the formation of covalently linked FTO-nucleic acids complexes. We were interested in non-mRNA CLIP-targeted RNA species and examined the potential activity of FTO on those RNA species. We first assessed the effect of FTO knockdown or overexpression on the total m^6A levels in mature rRNA (Figure S4B) in HeLa, HEK293T, and 3T3-L1 cell lines, respectively. No significant changes were observed for m^6A in purified mature rRNAs, including 28S rRNA (Figure S4C) and 18S rRNA (Figure S4D). We also compared the m^6A levels of top snRNA targets revealed by CLIP-

seq, including U1 RNA (a complex band of U1 RNA and 5.8S, Figure S4E), U2 RNA, and U6 RNA, in *Fto* homozygous knockout (*Fto*$^{-/-}$) MEF *versus* the wild-type MEF cells. Interestingly, we observed increased m^{6}A in the U6 RNA (Figure 4B) but not other snRNAs (Figure S4F) with the depletion of Fto in the *Fto*$^{-/-}$ compared with the wild-type MEF cells, suggesting that U6 m^{6}A could be demethylated by FTO.

Besides m^{6}A, we also tested FTO demethylation of m^{6}A$_m$ in these U RNAs. After decapping, increased m^{6}A$_m$ was observed in both U1/5.8s RNA and U2 RNA (Figure 4C). The quantification results showed a reasonable level of m^{6}A$_m$ in U2 RNA, with close to one m^{6}A$_m$ per U2 RNA molecule (187 bp long). To determine if the m^{6}A$_m$ is near the cap or internal, we measured the internal m^{6}A$_m$ level without decapping; decapping is required to remove the cap structure and expose cap m^{6}A$_m$ before nuclease P1 and alkaline phosphatase digestion. Internal m^{6}A$_m$ was also observed in both U2 and U1/5.8S RNA (Figure 4D), with increased internal m^{6}A$_m$ observed in U1/5.8s RNA in the *Fto*$^{-/-}$ compared to the wild-type MEF cells. However, considering the average length of mammalian U1 snRNA and 5.8s rRNA (around 160 bp), the 0.1% ratio of internal m^{6}A$_m$/A indicates less than 0.05 m^{6}A$_m$ per molecule of U1 snRNA. In U2 RNA both the cap and internal m^{6}A$_m$ modifications are more abundant, approaching to 0.5 per molecule of U2 RNA, respectively. The *Fto* knockout led to a significant increase of the total m^{6}A$_m$ level, most likely at the cap. Given the role of snRNPs in the splicing of mRNA (Maniatis and Reed, 1987), and previous work suggesting that FTO deficiency promotes splicing (Zhao et al., 2014), it will be interesting to investigate this potential link between FTO-induced modification changes in snRNAs and mRNA splicing in the future.

FTO Mediates m^{1}A Demethylation in tRNA

In the CLIP-seq results, we observed that FTO associates with tRNA and the distribution of CLIP reads in tRNA is significantly enriched compared to input (Table S2 and Table S3). We found that the knockdown of FTO led to the increase of 14.7%, 26.5%, and 38.1% of the total m^{1}A level in tRNA (Figure 5A) compared with the knockdown control in HeLa, HEK293T, and 3T3-L1 cells, respectively. The transcript levels of ALKBH1 and ALKBH3, which were previously shown to mediate tRNA m^{1}A demethylation (Liu et al., 2016; Ueda et al., 2017), remain unchanged upon the knockdown of FTO (Figure S5A) (Mauer et al., 2017), The overexpression of ΔNLS-FTO led to the opposite effects with about 19.6%, 23.1%, and 20.4% decrease of m^{1}A in tRNA observed (Figure 5B) when compared with controls in HeLa, HEK293T, and 3T3-L1 cells, respectively. We then separated the nuclear and cytoplasmic fractions of HEK293T cells with FTO knocked down *versus* the control. Both nuclear tRNA m^{1}A and cytoplasmic tRNA m^{1}A increased upon FTO knockdown, with cytoplasmic tRNA m^{1}A showing a larger increase (Figure 5C).

Interestingly, the m^{1}A level in tRNA is dramatically affected by FTO-mediated demethylation in comparison to m^{6}A and cap m^{6}A$_m$ in polyadenylated RNAs in *Fto* knockout mouse cells and tissues. In *Fto*$^{-/-}$ MEF cells, we observed a significant increase of the total m^{1}A in tRNA with no noticeable differences of m^{6}A or m^{6}A$_m$ in polyadenylated RNAs observed (Figure 5D). Both nuclear tRNA m^{1}A and cytoplasmic tRNA m^{1}A showed noticeable increases in *Fto*$^{-/-}$ MEF cells compared with the wild-type MEF cells (Figure

5E). The separation of nucleus and cytoplasm for MEF cells was validated by western blot (Figure S5B) and qRT-PCR (Figure S5C). We further tested the changes of the m^1A levels in tRNA as well as m^6A and cap m^6A_m in polyadenylated RNAs in the brain tissue of *Fto*$^{-/-}$ mice (Figure S5D). While the total m^6A and m^6A_m showed slight increases in five pairs of *Fto*$^{-/-}$ *versus* the wild-type mouse brains, the total m^1A level in tRNA showed the largest increases in the brain of the *Fto*$^{-/-}$ mice (Figure 5F). It is possible that the surviving *Fto* knockout mice have adapted to the loss of *Fto* with compensated changes of the total m^6A or cap m^6A_m levels in polyadenylated RNA. Many of these knockout mice still die early (several weeks after birth) in our hands, suggesting the lack of demethylation of individual mRNA or other RNA species still exhibits a noticeable effect on these mice. We also tested the level changes of m^1A in tRNA in two cell lines related to human leukemia. Stable knockdown of FTO leads to significantly increased tRNA m^1A in NB4 and MONOMAC-6 cells (Figure S5E).

We examined whether FTO exhibits biochemical demethylation activity towards m^1A in tRNA by treating the purified total tRNA from HEK293T cells with the FTO protein under reported demethylation conditions. The levels of abundant tRNA methylations, including m^1A, m^1G, m^7G, and m^5C, m^2G, $m^2{}_2G$, A_m, and m^3C, were measured in the presence or absence of EDTA. Incubation of purified tRNA with FTO led to a dramatic decrease of the m^1A level (Figure 5G), and a slight decrease of m^3C, but not levels of other modifications (Figure S5F), in comparison to the control samples, confirming that m^1A in tRNA is a biochemically viable substrate of FTO in addition to m^6A and m^6A_m in the polyadenylated RNAs. We then compared the demethylation activity of FTO towards tRNA m^1A and mRNA m^6A by incubating similar numbers of m^1A and m^6A together with FTO in the presence or absence of EDTA. The demethylation activity of FTO towards tRNA m^1A is lower than that of polyadenylated RNA m^6A (Figure S5G). However, considering the abundances of tRNA and polyadenylated RNA inside mammalian cells, the demethylation towards tRNA m^1A could still be functionally important.

m^1A58 is the most common m^1A site in tRNA, residing in the loop region of a TΨC stem-loop motif of tRNA (Hopper and Phizicky, 2003; Phizicky and Hopper, 2010), and can be reversed through demethylation in HeLa and MEF cells (Liu et al., 2016). We reasoned that FTO may preferentially mediate m^1A demethylation in tRNAs with a selectivity towards a stem-loop structure, as previous studies suggested low activities of FTO towards m^1A in single-stranded nucleic acid substrates (Jia et al., 2008). We synthesized two ssRNA probes, one with m^1A in a stem-loop sequence mimicking the TΨC loops in $tRNA^{His(GUG)}$ (contains m^1A58) and the other one with m^1A in an unstructured sequence (Figure S5H). Indeed, FTO exhibited low activity towards m^1A in the unstructured probe but a high preference for the stem-loop probe (Figure S5I). This biochemical result, combined with the quantifications of modification changes in various cells and tissues, support m^1A in tRNA as another substrate of FTO.

We asked why FTO could have distinct RNA species as demethylation substrates especially the preference for the loop structure. We examined the published protein structures and realized the unique structural features of FTO that allow it to gain access to the modification sites in multiple RNA species. We noticed that the overall structure of FTO has similarities

with NSUN6, a tRNA m^5C methyltransferase (Haag et al., 2015). In the overlapped structures of FTO and NSUN6 with bound tRNA, we observed that the FTO active site could gain access to tRNA m^1A58 (Figure S5J, left: overlapped structures of FTO (raspberry) with the complex of NSUN6 (purple) and tRNA (orange), with the iron center depicted in a yellow ball). However, another known mRNA m^6A demethylase, ALKBH5, does not carry the similar structural fold as FTO does, which may explain the more constrained substrate specificity of ALKBH5 on mRNA m^6A (Figure S5J, right: overlapped structures of ALKBH5 (green) with the complex of NSUN6 (blue) and tRNA (orange)).

FTO-mediated tRNA Demethylation Affects Translation

We further validated the m^1A demethylation activity of FTO on selected target tRNAs (Figure 6A). Biotin-labeled DNA probes complementary to tRNA species were used to specifically isolate the corresponding tRNA from 3T3-L1 cells. The m^1A level of the purified specific tRNA was then measured using LC-MS/MS. The results demonstrated that the knockdown of FTO leads to consistent increases of the m^1A levels in most top confident tRNAs targets bound to FTO, including $tRNA^{Glu(CUC)}$, $tRNA^{His(GUG)}$, $tRNA^{Gly(GCC)}$, $tRNA^{Gly(ACC)}$, $tRNA^{Asp(GUC)}$, $tRNA^{Lys(CUU)}$, $tRNA^{Gln(CUG)}$, and $tRNA^{Leu(CAA)}$ (Figure 6B). In addition, we also tested several tRNAs that were not FTO targets according to our FTO CLIP-seq data, including $tRNA^{Ala(AGC)}$, $tRNA^{Asn(GUU)}$, $tRNA^{Gly(UCC)}$, and $tRNA^{Phe(GAA)}$. Results revealed that FTO does not exhibit enzymatic activity on these non-targeted tRNAs (Figure S6A). Therefore, the majority of tRNAs identified by CLIP-seq are substrates of FTO.

We then used an alkyne-modified glycine analog, L-homopropargylglycine (HPG), to metabolically label newly synthesized proteins in *Fto*$^{-/-}$ and wild-type MEF cells. The HPG-labeled cells were then fluorescently labeled and analyzed by flow cytometry. The results showed a notable increase in the protein synthesis in the *Fto*$^{-/-}$ cells compared to the wild-type cells (Figure 6C and Figure S6B).

To separate the effects of the FTO-mediated tRNA m^1A demethylation from the effects of the FTO-mediated adenosine demethylation in mRNA on translation, we performed an *in vitro* translation assay by using a rabbit reticulocyte-based luciferase reporter system (Promega). tRNAs extracted from *Fto*$^{-/-}$ and wild-type MEF cells were subjected to the *in vitro* luciferase mRNA translation assay using rabbit reticulocyte lysate, respectively. The activity of the translated luciferase protein was measured in the incubation mixture by a luminometer. As shown in Figure 6D, the incubation of tRNAs extracted from *Fto*$^{-/-}$ cells induced significantly higher luciferase signals than tRNAs extracted from the wild-type MEF cells, indicating that the FTO-mediated tRNA demethylation led to increased protein translation efficiency.

We further designed a reporter assay with six repeated codon sequences (6×GAG(Glu) for $tRNA^{Glu(CUC)}$ target and 6×CAC(His) for $tRNA^{His(GUG)}$ target) added to the 5' of firefly luciferase (F-luc) (Figure 6E, left); a second *Renilla* luciferase (*R*-luc) encoded in the same plasmid was used to normalize the expression efficiency. For both reporters, the significantly elevated translation was observed in the *Fto*$^{-/-}$ MEF cells compared to the wild-type MEF cells (Figure 6E, right). We also applied a reporter assay with six repeated codon sequences

(6×GGA(Gly)) for non-target $tRNA^{Gly(UCC)}$ to the same reporter system mentioned above as the negative control. As expected, there was no noticeable change of translation between *Fto*$^{-/-}$ MEF cells and the wild-type MEF cells (Figure S6C). These results further indicate that the FTO-mediated tRNA m^1A demethylation negatively affects translation, which is consistent with the previous discovery that m^1A-methylated tRNAs are preferentially recognized and delivered to translation-active polysomes (Liu et al., 2016).

Discussion

FTO harbors two structural domains, an *N*- and a *C*-terminal domain. The active site of FTO resides in its *N*-terminal domain and is exposed to the protein surface (Han et al., 2010). Unlike ALKBH1, which possesses a distinct tRNA-binding domain (Liu et al., 2016), FTO contains an L1-loop surrounding its active site across to the Jelly-roll motif on the other side of the active site. The L1-loop facilitates FTO's selectivity towards single-stranded RNA substrates. The additional *C*-terminal domain, which is absent in the other AlkB family proteins (Yang et al., 2008; Yu et al., 2006), may endow FTO with the ability to associate with potential protein partners. These structural features may allow FTO to accomplish demethylation of different RNA substrates *via* interacting with diverse partner proteins depending on the cellular context.

Demethylation of m^6A and Cap m^6A_m in mRNA by FTO in the Nucleus and Cytoplasm

Both internal m^6A and cap m^6A_m exist in polyadenylated RNA in mammalian cells. The levels of internal m^6A are about 10–20 folds higher than those of cap m^6A_m in different cell lines (Wei et al., 1975a; Wei et al., 1975b). Our cellular results and biochemical assays using FTO and purified mRNA unequivocally show demethylation of both internal m^6A and cap m^6A_m by FTO. While FTO catalyzes more potent demethylation on cap m^6A_m over m^6A *in vitro*, the extent of demethylation inside cells is opposite with 5–10 folds more m^6A demethylated by FTO compared with m^6A_m in cell lines tested, in absolute terms. The primary polyadenylated RNA substrate of FTO in the cell nucleus appears to be m^6A, with cap m^6A_m more a target of FTO in the cytoplasm (Figure 7).

Nuclear mRNAs consist of only a portion of total cellular mRNAs. A notable fraction of nuclear mRNAs or other polyadenylated RNAs are substrates of FTO-mediated demethylation. In HeLa cells, although FTO could impact a significant fraction of nuclear polyadenylated m^6A, this effect is "diluted" when examining the total mRNA pool. It should be noted that when FTO shuttles to the cytoplasm, it may still demethylate a portion of m^6A in cytoplasmic mRNAs as it could gain access to both internal m^6A and cap m^6A_m on mRNA (Figure 7). In certain AML cells, the cytoplasmic m^6A demethylation by FTO can affect almost 40% of the total m^6A (Figure S2H and Figure S2J). Because the total m^6A level is considerably higher than that of m^6A_m in mRNA, a change of the similar percentage of m^6A *versus* m^6A_m manifests as a much larger number of m^6A changes in mRNA.

Functional Relevance of Cap m^6A_m and Internal m^6 A Demethylation by FTO

A previous study showed that the presence of m^6 A_m adjacent to the 5' cap prevents decapping and stabilizes mRNA transcripts in HEK293T cells (Mauer et al., 2017). In order

to further probe the effect of m^6A_m, we categorized the previously identified transcripts (Mauer et al., 2017) into four classes: cap m^6A_m -only transcripts, m^6A_m-only transcripts, transcripts containing both modifications, and transcripts with neither modification. In HEK293T cells, m^6A-only transcripts showed increased transcript levels upon FTO knockdown (Figure 3A and 3B), suggesting the presence of mechanisms that stabilize m^6A-modification transcripts. The YTHDF2-mediated decay of methylated transcripts operates in HeLa cells (Ke et al., 2017; Zhao et al., 2014), but may not be the predominant pathway affecting the transcript levels of m^6A-containing transcripts in HEK293T and AML cells (Li et al., 2017).

To our surprise, when we analyzed cap m^6A_m-only transcripts, we found that FTO knockdown does not noticeably affect mRNA transcript levels of cap m^6A_m-only genes in reported HEK293T cells. A careful analysis indicated that the previous analysis combined cap m^6A_m-only transcripts with transcripts that contain both cap m^6A_m and m^6A (Mauer et al., 2017).

The transcript stabilizing effect is most likely derived from the internal m^6As that co-exist with cap m^6A_m in transcripts that contain both modifications. So far, all functional relevant reports of FTO have been ascribed to internal m^6A in mRNA, which include a wide range of different systems (Cui et al., 2017; Gokhale et al., 2016; Su et al., 2018; Xiang et al., 2017; Yu et al., 2018; Zhou et al., 2015; Zhou et al., 2018; Zou et al., 2016). A recently published FTO CLIP-seq result revealed a peak of FTO binding closely around known m^6A sites and in intronic regions in HEK cells, suggesting that FTO mediates intronic m^6A demethylation (Bartosovic et al., 2017).

The discoveries of the cap m^6A_m in stabilizing mRNA and its demethylation by FTO are interesting and could potentially open new research directions (Mauer et al., 2017); however, the effects of FTO on cap m^6A_m of these mRNA transcripts require future investigations. The methyltransferase will need to be identified and the phenotypes of the methyltransferase knockout cells or mice need to be investigated and compared to severe phenotypes observed in *Fto* knockout mice. The role of cap m^6A_m demethylation in RNA species other than mRNA merits consideration. Appropriate and sensitive detection method and procedures are critical to investigate the FTO-mediate demethylation in the future research of the community.

tRNA m^1A and Small Nuclear RNA Demethylation by FTO

CLIP-seq results of FTO followed by LC-MS/MS tests revealed additional substrates of FTO, including m^6A in U6 RNA (Figure 4B) as well as internal and cap m^6A_m in snRNA (Figure 4C and 4D). The demethylation towards modifications in these U RNAs may affect mRNA splicing. However, cautions must be taken as the ratio of m^6A/A or m^6A_m/A for these small nuclear RNAs ranges from 0.05–2%. For short RNA species such as U1 and U6, the very low modified A/A ratio (0.05–0.5%) indicated far below stoichiometric methylation with 0.02–0.2 m^6A_m or m^6A per snRNA molecule. Close to one m^6A_m, either at the cap or internal, exists per U2 RNA molecule, and the cap U2 m^6A_m demethylation by FTO can have functional consequences in splicing, as previously suggested (Maniatis and Reed, 1987; Zhao et al., 2014).

When comparing the modification levels in the *Fto*$^{-/-}$ mouse MEF cells and brain tissues with the wild-type control we observed a large change of m^{1}A in tRNA. m^{1}A methylation in tRNA is important for the cell viability and fitness (Oerum et al., 2017), with m^{1}A/A ratio ranging around 1–3%. Previous studies have shown that m^{1}A58 is installed by the methyltransferase complex Trmt6/61 (Anderson et al., 1998) and can be reversed by ALKBH1 (Liu et al., 2016). The dynamic regulation of tRNA m^{1}A58 could impact translation initiation and elongation. In the current study, our CLIP sequencing data showed that FTO binds m^{1}A58-containing tRNAs. Further biochemical characterization revealed that FTO possesses effective tRNA m^{1}A demethylation activity *in vitro* and inside cells (both nucleus and cytoplasm). In fact, FTO was originally shown to be able to reverse DNA 1mA damage in 2007 (Gerken et al., 2007), most likely on ssDNA (Jia et al., 2008). The reporter assay confirmed that the FTO-mediated tRNA demethylation affects translation, which is reminiscent of the mechanism used by ALKBH1 in regulating translation elongation. FTO mediates both nuclear and cytoplasmic m^{1}A demethylation in tRNA. The mRNA cap m^{6}A$_m$ demethylation (Mauer et al., 2017) and tRNA m^{1}A demethylation by FTO could collectively repress translation, with cap demethylation perhaps destabilizing mRNA in certain cells or growth conditions and tRNA demethylation reducing translation. The m^{1}A tRNA demethylation by FTO may also impact tRNA fragments during certain development processes, which merits further investigations.

In summary, we uncover a previously unrecognized spatial regulation of RNA demethylation through FTO with distinct roles in the cell nucleus *versus* cytoplasm. Internal m^{6}A is the primary target of nuclear FTO in most cells. FTO can be localized to the cytoplasm and mediate both m^{6}A and cap m^{6}A$_m$ demethylation in polyadenylated RNA (Figure 7). In certain AML cells, we observed dramatic (up to 40%) m^{6}A mRNA demethylation by FTO in the cytoplasm. FTO also mediates demethylation of m^{1}A in tRNA in both cell nucleus and cytoplasm, which may tune translation together with cytoplasmic cap m^{6}A$_m$ mRNA demethylation. Some of the phenotypes observed for FTO in brain tissues may be partially derived from tuning translation through tRNA demethylation. We also identified additional RNA substrates including m^{6}A and internal and cap m^{6}A$_m$ in snRNAs (Figure 7). The snRNA demethylation, in particular, m^{6}A$_m$ in U2 RNA, may contribute to effects on splicing (Zhao et al., 2014). Lastly, the nuclear-centralized m^{6}A demethylation and the ability of FTO to mediate m^{1}A demethylation suggest potential nuclear roles of the m^{6}A or m^{1}A demethylation, on both polyadenylated RNA and other nuclear RNA species, in affecting gene expression, which will be investigated in the future.

STAR METHODS

CONTACT FOR REAGENT AND RESOURCE SHARING

Further information and requests may be directed to and will be fulfilled by the lead contact corresponding author Chuan He (chuanhe@uchicago.edu).

EXPERIMENTAL MODEL AND SUBJECT DETAILS

Cell culture—Wild-type MEF (mouse embryonic fibroblasts) and *Fto*$^{-/-}$ MEF cell lines were obtained from Prof. Arne Klungland. Spontaneously immortalized clonal MEF cell

lines were established from individual E13.5-E15.5 days-old embryos obtained from heterozygous *Fto*$^{+/-}$ crossings. Limbs were removed and remaining tissue chopped into small pieces and homogenized into single-cell suspension using a pipette. MEFs are grown in DMEM with 10% serum, 2 mM glutamine and penicillin/streptomycin. Cells grown for 4–7 days were trypsinized and frozen in complete medium with 10% DMSO as stock. Cells are grown in complete medium for 2–4 days before using them for following analysis. Human HeLa, HepG2, HEK293T, Mel624, and 3T3-L1 cell lines were purchased from ATCC. The aforementioned cells were maintained in DMEM (Gibco, #11965) with 10% fetal bovine serum (FBS, Gibco, 10438–026) and 1× Pen/Strep (Gibco, 15140) at 37°C with 5% CO_2. FTO stable knockdown and the knockdown control AML cells were obtained from Prof. Jianjun Chen and cultured as previously reported (Li et al., 2017).

Tissues—Wild-type and *Fto*$^{-/-}$ mouse brains were obtained from Prof. Arne Klungland. Littermate animals were used as *Fto*$^{+/+}$ controls (wild-type). The mice were bred and housed in a 12-hour light/dark cycle at the Comparative Medicine, Oslo University Hospital, Rikshospitalet, Norway, with a diet of pellets and water ad libitum. Brains were carefully removed from decapitated mice and quickly frozen on dry ice and stored at −80°C.

METHOD DETAILS

Plasmid construction—FLAG-tagged human FTO in the pcDNA 3.0 vector was obtained as previously reported (Jia et al., 2011). FLAG-tagged mouse FTO in the pCMV6-Entry vector was purchased from OriGene (MR208064). FLAG-tagged human ΔNLS-FTO mutant in pCMV6-Entry was generated by the deletion of 17 amino acids from the *N*-terminal of FTO full-length cDNA. High-purity plasmids used for mammalian cell transfection were prepared using HiSpeed Plasmid Maxi Kit (QIAGEN).

siRNA knockdown, and plasmid transfection—AllStars negative control siRNA (Qiagen, 1027281) was used as control siRNA in knockdown experiments. siRNA directed against human FTO (used in HEK293T and HeLa cells) was ordered from Qiagen (SI04293625, Hs_FTO_7 FlexiTube siRNA). Silencer® Select against mouse FTO (used in 3T3-L1 cells) was ordered from ThermoFisher (assay ID 166879). Cells were resuspended 16 hours prior to the transfection and maintained at 50% confluency for siRNA transfection or 80% confluency for plasmid transfection. Transfection was achieved by using Lipofectamine RNAiMAX (Invitrogen) for siRNA and Lipofectamine 2000 (Invitrogen) for DNA plasmids, following the manufacturer's protocols, respectively. The cells were harvested after 48 hours post siRNA transfection or 24 hours post plasmid transfection for subsequent experiments.

Cytoplasm and nucleus separation—Cytoplasm and nucleus were separated using NE-PER® Nuclear and Cytoplasmic Extraction Reagents (Thermo Scientific, 78833) following the manufacturer's protocol. The capability of this kit to efficiently separate cytoplasm and nucleus for HEK293T cell and MEFs cell has been reported previously (Huang et al., 2017b; McKenna and Wright, 2015). According to the published protocol (Conrad and Ørom, 2017), the separation efficiency was validated using qRT-PCR for total RNA purified from different cellular fractions as well as western blot.

Immunofluorescent imaging sample preparation—Immunofluorescent imaging was performed as reported previously (Zhao et al., 2014). In brief, the cells were cultured in an 8-well chamber (Lab-Tek) after treatment indicated in each experiment. The cells were washed once in phosphate buffered saline (PBS) and then fixed in 4% paraformaldehyde in PBST (PBS with 0.05% Tween-20) at the room temperature for 15 min. The fixing solution was removed, and −20 °C chilled methanol was immediately added to each chamber. After incubated for 10 min at the room temperature, the cells were rinsed once with PBS and blocked with blocking solution (1% BSA with PBST) for 1 hour at the room temperature. After that, the blocking solution was replaced with the primary antibody (ab126605 for FTO, 1:1000 dilution in the blocking solution, identical to the previous report (Aas et al., 2017)) and incubated for 1 hour at room temperature. After being washed 4 times with PBST (300 μl, 5–10 min for each wash), secondary antibody (1:300 dilution in PBST) was added to the mixture and incubated at room temperature for 1 hour. After washing 4 times with PBST (300 μl, 5–10 min for each wash), anti-fade reagent (Slowfade, Invitrogen) was added to mount the slides.

RNA purification—Total RNA was purified with TRIzol® reagents (Thermofisher Scientific, #15596018) from cell lysate. Polyadenylated RNA was purified from total RNA with two rounds of polyA tail purification using Dynabeads® mRNA DIRECT™ kit (Thermofisher Scientific, #61006). The rRNAs was further removed using RiboMinus™ Eukaryote kit (Thermofisher Scientific, A1083708). Small RNAs (< 200 nt) were separated from total RNA and then subjected to size selection using 15% TBE-urea gel (Thermofisher Scientific, EC6885BOX). tRNA was then sliced and recovered from the gel.

For small nuclear RNAs, the nuclei were first isolated using aforementioned NE-PER kit and the total nuclear RNA was purified using TRIzol® reagents. Small nuclear RNAs (< 200 nt) were separated from total nuclear RNA and then subjected to size selection using 6% TBE-urea gel (Thermofisher Scientific, EC6865BOX). Individual small nuclear RNA was then sliced based on molecular weight and recovered from the gel.

Biotinylated single-stranded DNA probes: As previously reported (Liu et al., 2016), DNA probes were designed to complement with the 3’ gene sequences of $tRNA^{Glu(CUC)}$, $tRNA^{His(GUG)}$, $tRNA^{Gly(GCC)}$, $tRNA^{Gly(ACC)}$, $tRNA^{Asp(GUC)}$, $tRNA^{Lys(CUU)}$, $tRNA^{Gln(CUG)}$, and $tRNA^{Leu(CAA)}$, $tRNA^{Ala(rGC)}$, $tRNA^{Asn(GUU)}$, $tRNA^{Gly(UCC)}$, and $tRNA^{Phe(rAA)}$. The probes used for tRNA selection are listed in Table S4.

Individual tRNA isolation—As previously reported (Liu et al., 2016), Streptavidin-conjugated C1 magnetic Dynabeads (Invitrogen) were used for individual tRNA target isolation. 20 μl of RNase-free beads were washed once with buffer A (10 mM Tris-HCl, pH 7.5, 2 mM EDTA, 2 M NaCl), and finally resuspended in 20 μl of buffer A. Subsequently, 200 μM of biotinylated oligonucleotides in 20 μl of water were mixed with resuspended Dynabeads in buffer A and incubated at room temperature for 30 min. After the incubation, the oligonucleotide-coated Dynabeads were then washed for four times with buffer B (5 mM Tris-HCl, pH 7.5, 1 mM EDTA, 1 M NaCl) and equilibrated in 6× SSC solution (1× SSC is 0.15 M NaCl plus 0.015 M sodium citrate, pH 7.0). Total tRNA in 6× SSC solutions and the oligonucleotide-coated Dynabeads and were heated for 10 min at 75°C separately. The

tRNA and beads were mixed and incubated together at 75°C for another 10 min. Thereafter, the suspension was gently rotated at room temperature for 3 hours before washed, in succession, three times with 3× SSC, twice with 1× SSC, and several times with 0.1× SSC until the absorbance of the wash solution at 260 nm closed to zero. tRNA retained on the beads was eluted three times using RNase-free water.

Quantitative analysis of RNA modification levels—For the quantification of the m^6A and cap m^6A_m in polyadenylated RNA, purified polyadenylated RNA (described in the RNA purification section above) was further treated with RppH (NEB, M0356S) in NEB Thermopol buffer for 2 hours to remove the cap. 50 ng polyadenylated RNA after the removal of the cap, purified tRNA and purified snRNAs were digested by nuclease P1 (Sigma, N8630), respectively, in 20 l of buffer containing 25 mM NaCl and 2.5 mM $ZnCl_2$ for 1 h at 42 °C. Subsequently, 1 unit of alkaline phosphatase (Sigma, P5931) and NH_4HCO_3 (100 mM) were added and the sample was incubated for another 1 h at 37 °C. The samples were then filtered (0.22 m, Millipore) and injected into a C18 reverse phase column coupled online to Agilent 6460 LC-MS/MS spectrometer in positive electrospray ionization mode. The nucleosides were quantified by using retention time and the nucleoside to base ion mass transitions (268-to-136 for A; 296-to-150 for m^6A_m, 282-to-150 for m^6A and m^1A (retention times of 2.5 and 0.9 min, respectively)). Quantification was performed by comparing with the standard curve obtained from pure nucleoside standards running with the same batch of samples. The m^6A and m^6A_m levels were calculated as the ratio of m^6A and m^6A_m to A, respectively. The tRNA m^1A level was calculated as the ratio of m^1A to G.

Biochemistry assay of FTO activity *in vitro*—Similar to a previous report (Liu et al., 2016), the demethylation activity assay was performed in standard 20 μl of reaction buffer containing KCl (100 mM), $MgCl_2$ (2 mM), SUPERNase In (0.2 U/μl, life technology), L-ascorbic acid (2 mM), α-ketoglutarate (300 M), $(NH_4)_2Fe(SO_4)_2{\cdot}6H_2O$ (150 μM), and 50 mM of HEPES buffer (pH 6.5). For m^6A and m^6A_m in polyadenylated RNA, 200 ng polyadenylated RNA purified from HEK293T cells was incubated with 2 M FTO purified in mammalian cells (High concentration) or 0.2 M FTO (low concentration) in the above reaction buffer for 3 hours and then quenched by the addition of 5 mM of EDTA, respectively. For tRNA m^1A, 200 ng tRNA purified from HEK293T cell was incubated with 2 M FTO purified in mammalian cells in the aforementioned reaction buffer for 3 hours and then quenched by the addition of 1 mM of EDTA. Excessive amount of EDTA was added to control samples. To incubate similar amounts of m^1A and m^6A with FTO, 100 ng purified mammalian polyadenylated RNA and 20 ng tRNA were pooled together and reacted under the aforementioned demethylation conditions; tRNA m^1A/A ratio is around 2–4% while polyadenylated RNA m^6AA ratio is around 0.4–0.8%. The RNAs were then isolated with 100 μl TRIzol® reagents (Thermofisher Scientific, #15596018) using standard protocol and subjected to RNA digestion prior to LC-MS/MS analysis.

Biochemical demethylation assays of FTO towards m^1A in single-stranded RNA (ssRNA) were conducted in 20 μl of reaction mixture together with 2 M FTO purified from the mammalian cells and 100 ng probes. The reaction was incubated at 37°C for 1 h and quenched by addition of 5 mM of EDTA. Excessive amount of EDTA was added to control

samples. The samples were then centrifuged at 16000 *g* for 30 min at 4°C. The supernatant was collected for RNA digestion prior to LC-MS/MS analysis. The sequences of the probes were listed in the STAR Method.

Luciferase reporter assay—The luciferase activity was measured by the luminometer (SYNERGY|HTX) following the manufacturing settings of luciferase reporter assay.

Similar to a previous report (Ueda et al., 2017), *in vitro* translation reaction was performed using the Flexi® Rabbit Reticulocyte Lysate System (Promega, L4540). Total tRNA purified from wild-type MEF cell and $Fto^{-/-}$ MEF cell was incubated for 30 min at 30°C with the reaction mixture following the manufacturing protocol.

For luciferase reporter inside cells, $tRNA^{His(GUG)}$ reporter was obtained as previously reported (Liu et al., 2016). Similarly, F-luc-6 × Glu(CAC) and F-luc-6 × Gly(UCC) reporter plasmid were obtained by inserting the sequence of GAGGAGGAGGAGGAGGAG and GGAGGAGGAGGAGGAGGA, respectively, before the F-luc coding region. To normalize translation differences between $Fto^{-/-}$ and wild-type MEF cells introduced by any other factors including initiation (*i.e.* variations of cellular levels of $tRNA^{iMet}$ and other tRNAs), a control reporter (F-luc plus *R*-luc) devoid of these 6× sequences was also transfected. The normalization factor from this control reporter was applied to signals obtained from the 6×GAG(Glu)-reporter, 6×CAC(His)-reporter, and 6×UCC(Gly)-reporter. General protocol: The wild-type and $Fto^{-/-}$ MEF cells were maintained in the 6-well plates at 80% confluency. 500 ng of reporter plasmids (pmirGlo empty vector as control or pmirGlo-specific tRNA anti-codon inserted vector) were transfected into wild-type and $Fto^{-/-}$ MEF cells following the aforementioned plasmid transfection protocol. After 6 hours, each well was each well was trypsin-digested, extensively washed with PBS, and re-seeded into a 96-well plate. After 18 hours from re-seeding, the cells in the 96-well plate were assayed using Dual-Glo® Luciferase Assay System (Promega, E2920). *Renilla* Luciferase (*R*-luc) was used to normalize firefly luciferase (F-luc) activity to evaluate the translation efficiency of the reporter.

Measurement of protein synthesis rate—HPG (Life Technologies; 50 nM final concentration) was added to the culture medium and incubated for 1 h. Cells were then lifted from plates and washed twice with phosphate buffered saline (PBS) and then fixed in 0.5 ml of 1% paraformaldehyde (Affymetrix) in PBS for 15 min on ice followed by permeabilizing in 200 μl PBS supplemented with 3% FBS (Sigma) and 0.1% saponin (Sigma) for 5 min at room temperature. The azide-alkyne reaction was performed with the Click-iT Cell Reaction Buffer Kit (Life Technologies) and azide-modified Alexa Fluor 488 (Life Technologies) at 5 mM final concentration. After a 30-minute reaction, the cells were washed twice with 3% BSA. All cells were filtered through a 40-μm cell strainer to obtain single cell suspensions. For flow cytometric analysis, all sorted fractions were double sorted to ensure high purity. Data were analyzed by FlowJo (Tree Star) software.

CLIP-seq—Similar to a previous report (Liu et al., 2016), in brief, for each cell line, 5 plates of cells in 15 cm style dish were grown until 80% confluency (~10^7 cells). The medium was aspirated and the cells were washed with PBS once and irradiated once with

400 mJ/cm2 at 254 nm in Stratalinker on ice. After irradiation, cells were harvested with a scraper, transferred to a microtube, pelleted at 4000 rpm for 3 min at 4°C, and then lysed in RIPA lysis buffer (Sigma, R2078) with cOmplete™, Mini, EDTA-free Protease Inhibitor Cocktail and SUPERNase In at 4°C for 4 hours. Subsequently, the lysis mixture was centrifuged at 17,000 g at 4°C for 30 min and the supernatant was carefully collected. Meanwhile, add 100 μl Anti-FLAG® M2 Magnetic Beads to a fresh microtube, wash beads twice with 1 ml lysis buffer. Change to a new tube, leave the beads in last wash until IP experiment. 100 μl of Anti-FLAG® M2 Magnetic Beads was added into the supernatant and mixed gently at 4°C for 4 hours. The supernatant was then discarded and the beads were washed for 3 times with 1 ml of high salt buffer and another 8 times with 1 ml of wash buffer (Wang et al., 2009). The RNAs were then eluted by proteinase K digestion following the manufacturer's protocol. Subsequently, RNAs were recovered by phenol/chloroform extraction and then subjected to library preparation using NEBNext® Multiplex Small RNA Library Prep Set for Illumina® (NEB, E7300S).

CLIP samples were pooled and sequenced with Hiseq-2000. Raw reads from CLIP samples were first trimmed according to recommended settings (Bolger et al., 2014). Gene structure annotations were downloaded from UCSC mm10 RefSeq/Repeatmasker. For CLIP-seq, we used a modified version of PARalyzer (Corcoran et al., 2011) to allow for all mutations, rather than just T to C mutations. For tRNA, the reads in each tRNA gene were counted. Similar to the previous report (Bartosovic et al., 2017), RNA-seq with rRNA depletion for 3T3-L1 was reanalyzed and used as the input for CLIP-seq (Schick et al., 2015). The reads distribution in tRNA of input (RNA-seq) in 3T3-L1 cells were shown in Table S2. The CLIP-seq in HEK293T cells was reanalyzed (Bartosovic et al., 2017). The reads distribution in tRNA of CLIP-seq and input (RNA-seq) in HEK293T cells were shown in Table S3.

Classification of the m^6A and m^6A_m only genes—The m^6A_m list was obtained from supplementary table 1 in the previous study (Mauer et al., 2017). The m^6A list was obtained from table S6 in the previous report (Meyer et al., 2012). In the reported m^6A list, the peak site was annotated. The genes containing both m^6A and m^6A_m were first classified by the overlap of two lists followed by deducting the genes that have m^6A in 5'UTR (though there must be some over deduction in this step as definitely not all the 5'UTR m^6As are m^6A_m, but just to be on the safe side). m^6A only genes were classified by deducting genes containing both m^6A and m^6A_m mentioned above from the genes in 2012 list. Similarly, cap m^6A_m only genes were classified by deducting genes containing both m^6A and m^6A_m mentioned above from the genes in 2017 list. The list of three groups of genes was provided in Table S1.

Replication—For the quantification of modification changes using LC-MS-MS: 6 replicates (RNAs were purified from three plates of cells each time and two rounds of experiments were performed) were tested for most samples of transient knockdown or overexpression and controls; 4 replicates (RNAs were purified from two plates of cells each time and two rounds of experiments were performed) were tested for samples with *Fto* knockout, wild-type or FTO stable knockdown and controls; 5 replicates (RNAs from five $Fto^{-/-}$ and wild type brains, respectively) were tested for the mouse brain samples of *Fto*

knockout and wild-type; and 3 replicates were tested for the individual tRNAs purified from *Fto*$^{-/-}$ and wild-type MEF cells. For the reporter assay experiments: *in vitro*, 8 replicates were performed (tRNAs were purified from four plates of cells each time and two rounds of experiments were performed); inside cells, 8 replicates were performed (cells were seeded in eight wells parallelly in one 96-well plate). For the HPG incorporation experiment, 3 replicates (three plates of cells) were tested.

QUANTIFICATION AND STATISTICAL ANALYSIS

P values were determined using the two-tailed Student's unpaired t-test for unpaired samples in LC-MS/MS results, protein synthesis results, and reporter results. *p < 0.05, **p < 0.01, ***p < 0.001, ****p < 0.0001. Error bars represent mean ± s.d.. *n.s.* means not significant, n = 3 for experiments in the Figure 5G, 6B, 6C, S4C, S4D, S5F, S5G, S5I, and S6A; n = 4 for experiments in the Figure 1B, 2C, 5A to 5E, S2G to J, and S5E; n = 5 for experiments in Figure 5F; n = 6 for experiments in Figure 2B, 4B to 4D, S1C to S1E, S2B to S2D, S3D, and S4F; n = 8 for experiments in Figure 6D, 6E and S6C. *P* values were determined using the Wilcoxon test in expression level analysis and using Mann-Whitney test in cumulative fraction results. *p < 0.05, **p < 0.01, ***p < 0.001, ****p < 0.0001. Error bars represent mean ± s.d.. *n.s.* means not significant, for n = transcript numbers in Figure 3 and Figure S3.

DATA AND SOFTWARE AVAILABILITY

Data resources—Sequencing data have been deposited into the Gene Expression Omnibus (GEO) under the accession number GSE106395.

Supplementary Material

Refer to Web version on PubMed Central for supplementary material.

ACKNOWLEDGEMENTS

This work is supported by the National Institute of Health (GM071440 and HG008935 to C.H., and CA214965 to J.C.) and the National Basic Research Program of China (2014CB964900). The Mass Spectrometry Facility of the University of Chicago is funded by National Science Foundation (CHE-1048528). The University of Chicago Cancer Center is supported by National Institute of Health CA014599. C.H. is an investigator of the Howard Hughes Medical Institute.

REFERENCE

Aas A, Isakson P, Bindesboll C, Alemu EA, Klungland A, and Simonsen A (2017). Nucleocytoplasmic Shuttling of FTO Does Not Affect Starvation-Induced Autophagy. PLoS One 12, e0168182. [PubMed: 28288181]

Adams JM, and Cory S (1975). Modified nucleosides and bizarre 5[prime]-termini in mouse myeloma mRNA. Nature 255, 28–33. [PubMed: 1128665]

Anderson J, Phan L, Cuesta R, Carlson BA, Pak M, Asano K, Bjork GR, Tamame M, and Hinnebusch AG (1998). The essential Gcd10p-Gcd14p nuclear complex is required for 1-methyladenosine modification and maturation of initiator methionyl-tRNA. Genes & Development 12, 3650–3662.

Bartosovic M, Molares HC, Gregorova P, Hrossova D, Kudla G, and Vanacova S (2017). N6-methyladenosine demethylase FTO targets pre-mRNAs and regulates alternative splicing and 3'-end processing. Nucleic Acids Res 45, 11356–11370. [PubMed: 28977517]

Boissel S, Reish O, Proulx K, Kawagoe-Takaki H, Sedgwick B, Yeo GS, Meyre D, Golzio C, Molinari F, Kadhom N, et al. (2009). Loss-of-function mutation in the dioxygenase-encoding FTO gene

causes severe growth retardation and multiple malformations. Am J Hum Genet 85, 106–111. [PubMed: 19559399]

Bolger AM, Lohse M, and Usadel B (2014). Trimmomatic: a flexible trimmer for Illumina sequence data. Bioinformatics 30, 2114–2120. [PubMed: 24695404]

Cecil JE, Tavendale R, Watt P, Hetherington MM, and Palmer CN (2008). An obesity-associated FTO gene variant and increased energy intake in children. N Engl J Med 359, 2558–2566. [PubMed: 19073975]

Church C, Moir L, McMurray F, Girard C, Banks GT, Teboul L, Wells S, Bruning JC, Nolan PM, Ashcroft FM, et al. (2010). Overexpression of Fto leads to increased food intake and results in obesity. Nat Genet 42, 1086–1092. [PubMed: 21076408]

Conrad T, and Ørom UA (2017). Cellular Fractionation and Isolation of Chromatin-Associated RNA In Enhancer RNAs: Methods and Protocols, Ørom UA, ed. (New York, NY: Springer New York), pp. 1–9.

Corcoran DL, Georgiev S, Mukherjee N, Gottwein E, Skalsky RL, Keene JD, and Ohler U (2011). PARalyzer: definition of RNA binding sites from PAR-CLIP short-read sequence data. Genome Biol. 12, R79 [PubMed: 21851591]

Cui Q, Shi H, Ye P, Li L, Qu Q, Sun G, Sun G, Lu Z, Huang Y, Yang CG, et al. (2017). m(6)A RNA Methylation Regulates the Self-Renewal and Tumorigenesis of Glioblastoma Stem Cells. Cell Rep 18, 2622–2634. [PubMed: 28297667]

Fawcett KA, and Barroso I (2010). The genetics of obesity: FTO leads the way. Trends Genet 26, 266–274. [PubMed: 20381893]

Fischer J, Koch L, Emmerling C, Vierkotten J, Peters T, Bruning JC, and Ruther U (2009). Inactivation of the Fto gene protects from obesity. Nature 458, 894–898. [PubMed: 19234441]

Fu Y (2012). Dynamic Regulation of Rna Modifications by AlkB Family Dioxygenases In Chemistry Department (Proquest, Order No. 3548228: The University of Chicago).

Fu Y, Dominissini D, Rechavi G, and He C (2014). Gene expression regulation mediated through reversible m(6)A RNA methylation. Nat Rev Genet 15, 293–306. [PubMed: 24662220]

Fu Y, Jia G, Pang X, Wang RN, Wang X, Li CJ, Smemo S, Dai Q, Bailey KA, Nobrega MA, et al. (2013). FTO-mediated formation of N6-hydroxymethyladenosine and N6-formyladenosine in mammalian RNA. Nat Commun 4, 1798. [PubMed: 23653210]

Gerken T, Girard CA, Tung YC, Webby CJ, Saudek V, Hewitson KS, Yeo GS, McDonough MA, Cunliffe S, McNeill LA, et al. (2007). The obesity-associated FTO gene encodes a 2-oxoglutarate-dependent nucleic acid demethylase. Science 318, 1469–1472. [PubMed: 17991826]

Gokhale NS, McIntyre ABR, McFadden MJ, Roder AE, Kennedy EM, Gandara JA, Hopcraft SE, Quicke KM, Vazquez C, Willer J, et al. (2016). N6-Methyladenosine in Flaviviridae Viral RNA Genomes Regulates Infection. Cell Host Microbe 20, 654–665. [PubMed: 27773535]

Gulati P, Avezov E, Ma M, Antrobus R, Lehner P, O'Rahilly S, and Yeo GS (2014). Fat mass and obesity-related (FTO) shuttles between the nucleus and cytoplasm. Biosci Rep 34, e00144. [PubMed: 25242086]

Haag S, Warda AS, Kretschmer J, Gunnigmann MA, Hobartner C, and Bohnsack MT (2015). NSUN6 is a human RNA methyltransferase that catalyzes formation of m5C72 in specific tRNAs. RNA 21, 1532–1543. [PubMed: 26160102]

Han Z, Niu T, Chang J, Lei X, Zhao M, Wang Q, Cheng W, Wang J, Feng Y, and Chai J (2010). Crystal structure of the FTO protein reveals basis for its substrate specificity. Nature 464, 1205–1209. [PubMed: 20376003]

He C (2010). Grand challenge commentary: RNA epigenetics? Nat Chem Biol 6, 863–865. [PubMed: 21079590]

Hess ME, Hess S, Meyer KD, Verhagen LA, Koch L, Bronneke HS, Dietrich MO, Jordan SD, Saletore Y, Elemento O, et al. (2013). The fat mass and obesity associated gene (Fto) regulates activity of the dopaminergic midbrain circuitry. Nat Neurosci 16, 1042–1048. [PubMed: 23817550]

Ho AJ, Stein JL, Hua X, Lee S, Hibar DP, Leow AD, Dinov ID, Toga AW, Saykin AJ, Shen L, et al. (2010). A commonly carried allele of the obesity-related FTO gene is associated with reduced brain volume in the healthy elderly. Proc Natl Acad Sci U S A 107, 8404–8409. [PubMed: 20404173]

Hopper AK, and Phizicky EM (2003). tRNA transfers to the limelight. Genes Dev 17, 162–180. [PubMed: 12533506]

Huang H, Weng H, Sun W, Qin X, Shi H, Wu H, Zhao BS, Mesquita A, Liu C, Yuan CL, et al. (2017a). Recognition of RNA N6-methyladenosine by IGF2BP Proteins Enhances mRNA Stability. Nat Chem Biol *under revision*.

Huang JH, Ku WC, Chen YC, Chang YL, and Chu CY (2017b). Dual mechanisms regulate the nucleocytoplasmic localization of human DDX6. Sci Rep 7, 42853. [PubMed: 28216671]

Jia G, Fu Y, Zhao X, Dai Q, Zheng G, Yang Y, Yi C, Lindahl T, Pan T, Yang Y-G, et al. (2011). N6-Methyladenosine in nuclear RNA is a major substrate of the obesity-associated FTO. Nat Chem Biol 7, 885–887. [PubMed: 22002720]

Jia G, Yang CG, Yang S, Jian X, Yi C, Zhou Z, and He C (2008). Oxidative demethylation of 3-methylthymine and 3-methyluracil in single-stranded DNA and RNA by mouse and human FTO. FEBS Lett 582, 3313–3319. [PubMed: 18775698]

Ke S, Pandya-Jones A, Saito Y, Fak JJ, Vagbo CB, Geula S, Hanna JH, Black DL, Darnell JE, Jr., and Darnell RB (2017). m(6)A mRNA modifications are deposited in nascent pre-mRNA and are not required for splicing but do specify cytoplasmic turnover. Genes Dev 31, 990–1006. [PubMed: 28637692]

Li Z, Weng H, Su R, Weng X, Zuo Z, Li C, Huang H, Nachtergaele S, Dong L, Hu C, et al. (2017). FTO Plays an Oncogenic Role in Acute Myeloid Leukemia as a N(6)-Methyladenosine RNA Demethylase. Cancer Cell 31, 127–141. [PubMed: 28017614]

Linder B, Grozhik AV, Olarerin-George AO, Meydan C, Mason CE, and Jaffrey SR (2015). Single-nucleotide-resolution mapping of m6A and m6Am throughout the transcriptome. Nat Methods 12, 767–772. [PubMed: 26121403]

Liu F, Clark W, Luo G, Wang X, Fu Y, Wei J, Wang X, Hao Z, Dai Q, Zheng G, et al. (2016). ALKBH1-Mediated tRNA Demethylation Regulates Translation. Cell 167, 816–828 e816. [PubMed: 27745969]

Maniatis T, and Reed R (1987). The role of small nuclear ribonucleoprotein particles in pre-mRNA splicing. Nature 325, 673–678. [PubMed: 2950324]

Mauer J, Luo X, Blanjoie A, Jiao X, Grozhik AV, Patil DP, Linder B, Pickering BF, Vasseur JJ, Chen Q, et al. (2017). Reversible methylation of m(6)Am in the 5' cap controls mRNA stability. Nature 541, 371–375. [PubMed: 28002401]

McKenna S, and Wright CJ (2015). Inhibiting IκBβ–NFκB signaling attenuates the expression of select pro-inflammatory genes. J Cell Sci 128, 2143–2155. [PubMed: 25908863]

Meyer KD, Saletore Y, Zumbo P, Elemento O, Mason CE, and Jaffrey SR (2012). Comprehensive analysis of mRNA methylation reveals enrichment in 3' UTRs and near stop codons. Cell 149, 1635–1646. [PubMed: 22608085]

Molinie B, Wang J, Lim KS, Hillebrand R, Lu Z. x., Van Wittenberghe N, Howard BD, Daneshvar K, Mullen AC, Dedon P, et al. (2016). m6A-LAIC-seq reveals the census and complexity of the m6A epitranscriptome. Nat Meth 13, 692–698.

Muller-McNicoll M, and Neugebauer KM (2013). How cells get the message: dynamic assembly and function of mRNA-protein complexes. Nat Rev Genet 14, 275–287. [PubMed: 23478349]

Oerum S, Degut C, Barraud P, and Tisne C (2017). m1A Post-Transcriptional Modification in tRNAs. Biomolecules 7, 20.

Phizicky EM, and Hopper AK (2010). tRNA biology charges to the front. Genes Dev 24, 1832–1860. [PubMed: 20810645]

Sanchez-Pulido L, and Andrade-Navarro MA (2007). The FTO (fat mass and obesity associated) gene codes for a novel member of the non-heme dioxygenase superfamily. BMC Biochem 8, 23. [PubMed: 17996046]

Schick S, Fournier D, Thakurela S, Sahu SK, Garding A, and Tiwari VK (2015). Dynamics of chromatin accessibility and epigenetic state in response to UV damage. J. Cell Sci. 128, 4380–4394. [PubMed: 26446258]

Su R, Dong L, Li C, Nachtergaele S, Wunderlich M, Qing Y, Deng X, Wang Y, Weng X, Hu C, et al. (2018). R-2HG Exhibits Anti-tumor Activity by Targeting FTO/m(6)A/MYC/CEBPA Signaling. Cell 172, 90–105 e123. [PubMed: 29249359]

Ueda Y, Ooshio I, Fusamae Y, Kitae K, Kawaguchi M, Jingushi K, Hase H, Harada K, Hirata K, and Tsujikawa K (2017). AlkB homolog 3-mediated tRNA demethylation promotes protein synthesis in cancer cells. Sci Rep 7, 42271. [PubMed: 28205560]

Van Nostrand EL, Pratt GA, Shishkin AA, Gelboin-Burkhart C, Fang MY, Sundararaman B, Blue SM, Nguyen TB, Surka C, Elkins K, et al. (2016). Robust transcriptome-wide discovery of RNA-binding protein binding sites with enhanced CLIP (eCLIP). Nat Methods 13, 508–514. [PubMed: 27018577]

Wang Z, Tollervey J, Briese M, Turner D, and Ule J (2009). CLIP: construction of cDNA libraries for high-throughput sequencing from RNAs cross-linked to proteins in vivo. Methods 48, 287–293. [PubMed: 19272451]

Wei C-M, Gershowitz A, and Moss B (1975a). N6, O2[prime]-dimethyladenosine a novel methylated ribonucleoside next to the 5[prime] terminal of animal cell and virus mRNAs. Nature 257, 251–253. [PubMed: 1161029]

Wei CM, Gershowitz A, and Moss B (1975b). Methylated nucleotides block 5' terminus of HeLa cell messenger RNA. Cell 4, 379–386. [PubMed: 164293]

Xiang Y, Laurent B, Hsu CH, Nachtergaele S, Lu Z, Sheng W, Xu C, Chen H, Ouyang J, Wang S, et al. (2017). RNA m(6)A methylation regulates the ultraviolet-induced DNA damage response. Nature 543, 573–576. [PubMed: 28297716]

Yang CG, Yi C, Duguid EM, Sullivan CT, Jian X, Rice PA, and He C (2008). Crystal structures of DNA/RNA repair enzymes AlkB and ABH2 bound to dsDNA. Nature 452, 961–965. [PubMed: 18432238]

Yu B, Edstrom WC, Benach J, Hamuro Y, Weber PC, Gibney BR, and Hunt JF (2006). Crystal structures of catalytic complexes of the oxidative DNA/RNA repair enzyme AlkB. Nature 439, 879–884. [PubMed: 16482161]

Yu J, Chen M, Huang H, Zhu J, Song H, Zhu J, Park J, and Ji SJ (2018). Dynamic m6A modification regulates local translation of mRNA in axons. Nucleic Acids Res 46, 1412–1423. [PubMed: 29186567]

Zhao X, Yang Y, Sun BF, Shi Y, Yang X, Xiao W, Hao YJ, Ping XL, Chen YS, Wang WJ, et al. (2014). FTO-dependent demethylation of N6-methyladenosine regulates mRNA splicing and is required for adipogenesis. Cell Res 24, 1403–1419. [PubMed: 25412662]

Zhou J, Wan J, Gao X, Zhang X, Jaffrey SR, and Qian S-B (2015). Dynamic m6A mRNA methylation directs translational control of heat shock response. Nature 526, 591–594. [PubMed: 26458103]

Zhou J, Wan J, Shu XE, Mao Y, Liu X-M, Yuan X, Zhang X, Hess ME, Brüning JC, and Qian S-B (2018). N6-Methyladenosine Guides mRNA Alternative Translation during Integrated Stress Response. Mol Cell 69, 636–647.e637. [PubMed: 29429926]

Zou S, Toh JDW, Wong KHQ, Gao Y-G, Hong W, and Woon ECY (2016). N6-Methyladenosine: a conformational marker that regulates the substrate specificity of human demethylases FTO and ALKBH5. Sci Rep 6, 25677. [PubMed: 27156733]

Highlights

1. FTO mediates both internal m^6A and cap m^6A_m demethylation of polyadenylated RNA
2. FTO exhibits differential substrate preferences in nucleus *versus* cytoplasm
3. The internal mRNA m^6A demethylation by FTO correlates with transcript level changes
4. FTO affects snRNA m^6A and m^6A_m levels and mediates tRNA m^1A demethylation

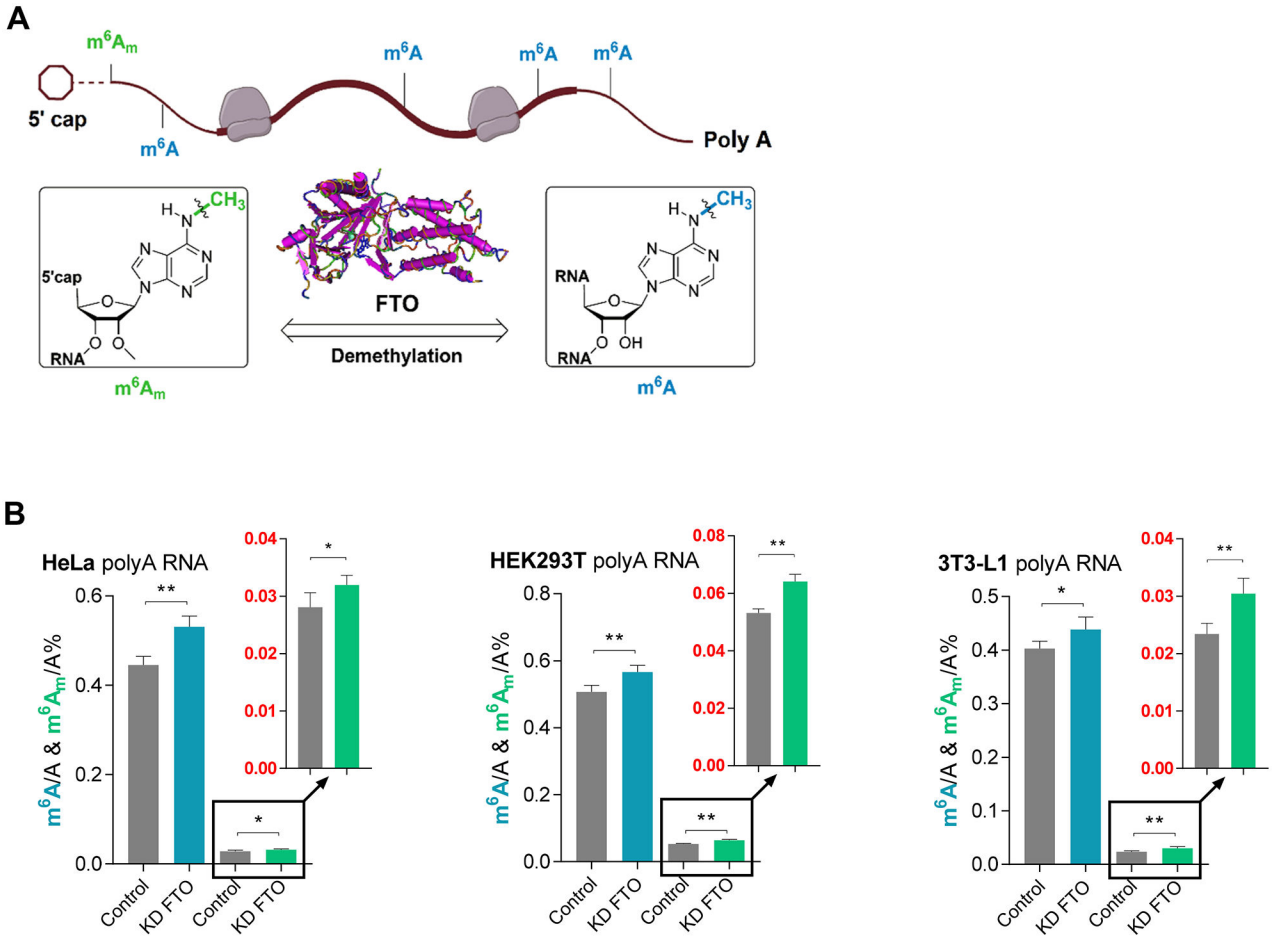

Figure 1. FTO Demethylates both m^6A and m^6A_m inside Cells.

See also Figure S1.

(A) A sketch that FTO mediates demethylation of m^6A and cap m^6A_m in polyadenylated RNA.

(B) Quantification of the m^6A/A and cap m^6A_m/A ratio in polyadenylated RNA by LC-MS/MS. In comparison to controls, significant increases in the m^6A/A ratio were consistently observed among HeLa, HEK293T, and 3T3-L1 cells upon transient knockdown of FTO (blue bars). Increases of the m^6A_m/A ratio were consistently observed among HeLa, HEK293T, and 3T3-L1 cells upon transient knockdown of FTO (green bars). *P* values were determined using Student's unpaired t-test. *p < 0.05, **p < 0.01, ***p < 0.001, ****p < 0.0001. *n.s.* means not significant. Error bars, mean ± s.d. for $n = 4$ experiments in (B).

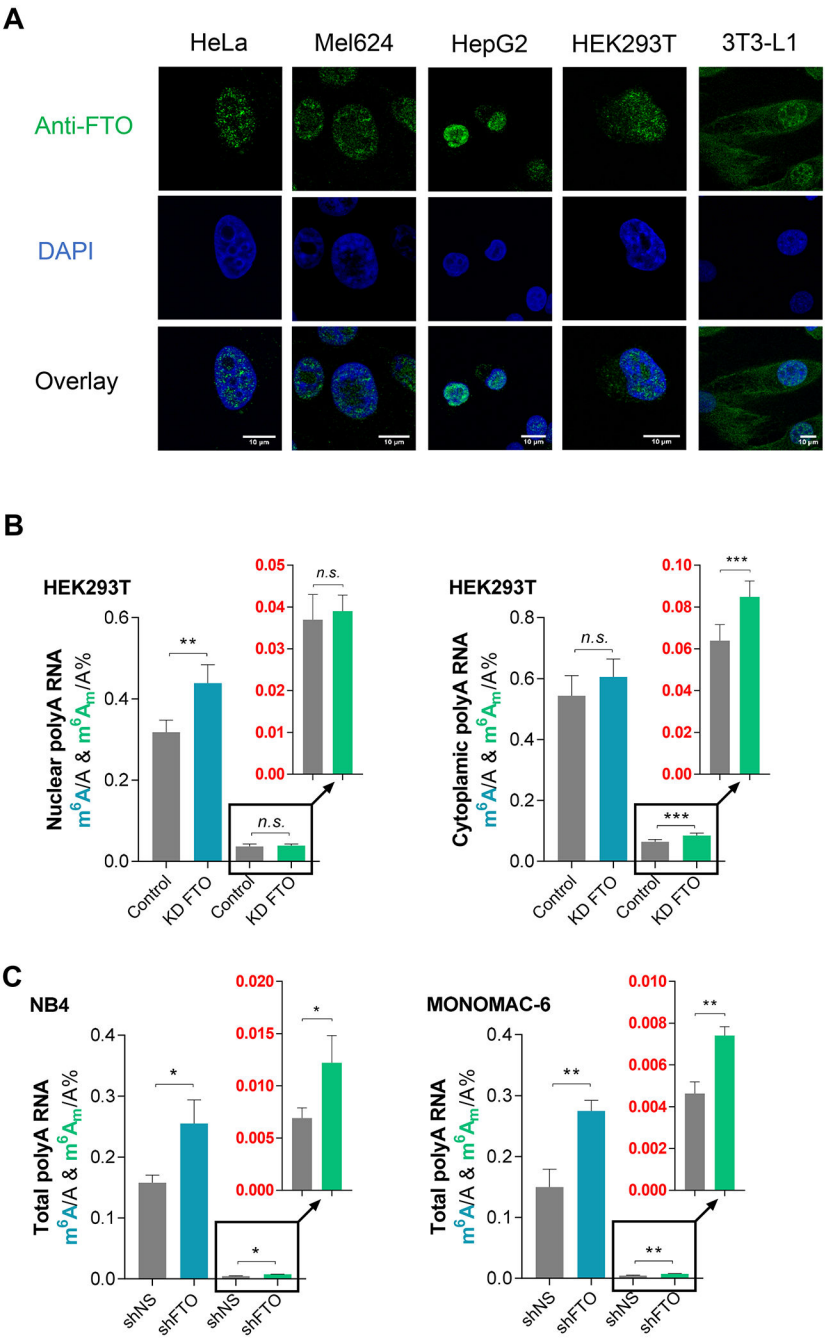

Figure 2. Subcellular Distribution of FTO Differs among Cell Lines and the Spatial Localization of FTO Influences its Demethylation of Target Substrates.

See also Figure S2.

(A) Subcellular localization of FTO (green) among HeLa, Mel624, HepG2, HEK293T, and 3T3-L1 cell lines. The nucleus was stained with DAPI (blue). Scale bar = 10 μm. Representative images are selected from three independent experiments.

(B) Quantification of the m^6A/A and cap m^6A_m/A ratios in polyadenylated RNA from HEK293T cells by LC-MS/MS. Transient knockdown of FTO led to a significant increase of nuclear polyadenylated RNA m^6A/A ratio but not the cytoplasmic polyadenylated RNA

m^6A/A ratio (blue bars). Transient knockdown of FTO led to a significant increase of cytoplasmic polyadenylated RNA m^6A_m/A ratio but no noticeable change of the nuclear polyadenylated RNA m^6A_m/A ratio (green bars).

(C) Quantification of the m^6A/A and cap m^6A_m/A ratios in polyadenylated RNA from NB4 cells (left) and MONOMAC-6 cells (right) by LC-MS/MS. Stable knockdown of FTO led to both increased m^6A/A and cap m^6A_m/A ratios in total polyadenylated RNA; *P* values were determined using Student's unpaired t-test. *p < 0.05, **p < 0.01, ***p < 0.001, ****p < 0.0001. *n.s.* means not significant. Error bars, mean ± s.d. for $n = 6$ experiments in (B); for $n = 4$ experiments in (C)

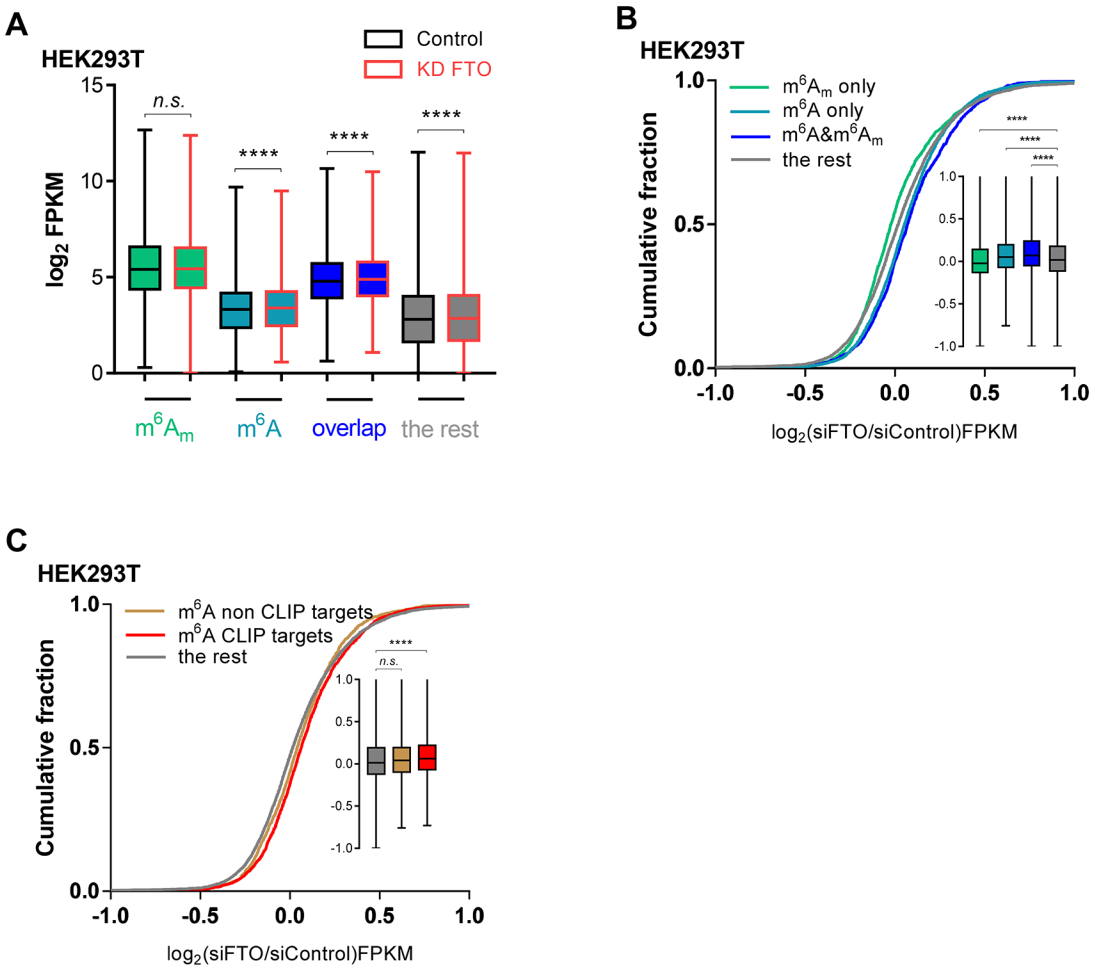

Figure 3. FTO-mediated Demethylation of m^6A but not m^6A_m in Polyadenylated RNA More Affects Transcript Expression Level Changes.

See also Figure S3 and Table S1.

(A) mRNA transcripts are classified into four groups: transcripts containing only m^6A_m, containing only internal m^6A, containing both m^6A and m^6A_m (overlap), and transcripts that contain neither m^6A nor m^6A_m (labeled as the rest). The global expression level of m^6A_m-alone transcripts did not significantly change upon FTO knockdown while the global transcript level of other three groups increased significantly.

(B) The cumulative fraction of gene expression shows that compared to the transcripts containing only m^6A, containing both m^6A and m^6A_m, and containing no m^6A or m^6A_m, the transcripts containing only m^6A_m but not m^6A showed significantly less transcript level change with FTO knockdown compared to the control (in A, *P* values were determined using the Wilcoxon test; in B, *P* values were determined using Mann-Whitney test. *p < 0.05, **p < 0.01, ***p < 0.001, ****p < 0.0001. *n.s.* means not significant. Error bars, mean ± s.d. for *n* = 3987, m^6A only; *n* = 2016, m^6A only; *n* = 1307, m^6 m A and m^6A_m; *n* = 5598, the rest).

(C) The cumulative fraction of gene expression shows that FTO CLIP targets showed significantly increased expression level upon transient knockdown of FTO but not non-targets for transcripts containing only m^6A compared to the rest genes. (In C, *P* values were determined using Mann-Whitney test. *p < 0.05, **p < 0.01, ***p < 0.001, ****p < 0.0001.

n.s. means not significant. Error bars, mean ± s.d. for $n = 1895$, m^6A genes overlapped with FTO targets; $n = 2092$, non-targets; $n = 8896$, the rest).

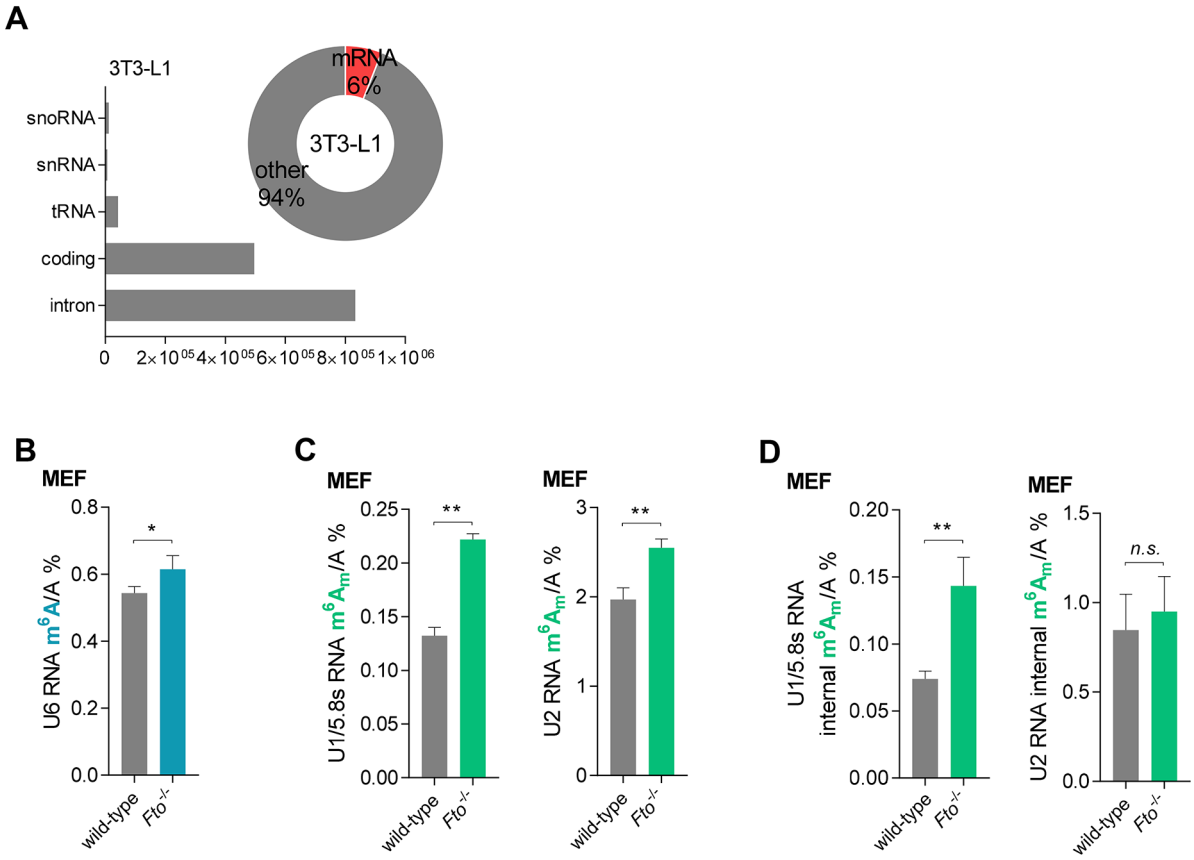

Figure 4. FTO-mediated Internal m^{6}A, Internal and Cap m^{6}A$_m$ Demethylation in snRNAs.

See also Figure S4.

(A) Bar graph summarizing the reads distribution of the FTO target RNA species in the 3T3-L1 cells; donut graph showing the percentage of the FTO-bound mRNA in all FTO CLIP-seq targets in the 3T3-L1 cell line.

(B) An increased m^{6}A/A ration in the U6 RNA was observed by LC-MS/MS in *Fto*$^{-/-}$ MEF cells compared to the control wild-type MEF cells.

(C) Quantification of the m^{6}A$_m$/A ratio of the U1/5.8s RNA and U2 RNA by LC-MS/MS after decapping, showing increased m^{6}A$_m$/A ratios in the *Fto*$^{-/-}$ MEF cells compared to the wild-type control.

(D) Quantification of the m^{6}A$_m$/A ratio in U1/5.8s RNA and U2 RNA by LC-MS/MS without decapping, showing increased internal m^{6}A$_m$/A ratios in *Fto*$^{-/-}$ MEF cells compared to the wild-type control. *P* values were determined using Student's unpaired t-test. *p < 0.05, **p < 0.01, ***p < 0.001, ****p < 0.0001. *n.s.* means not significant. Error bars, mean ± s.d. for *n* = 6 experiments in (B) to (D).

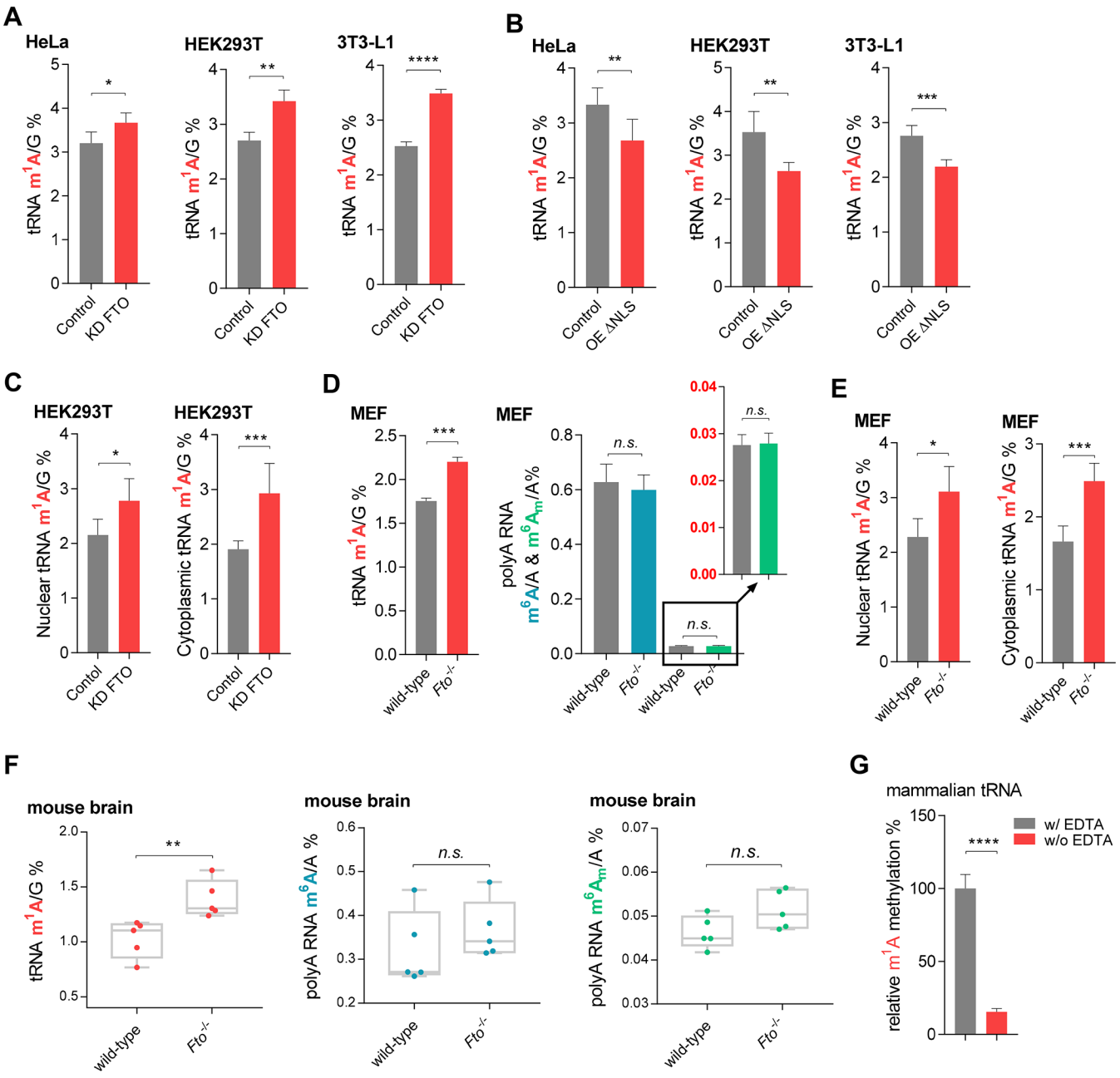

Figure 5. FTO-mediated tRNA m^{1}A Demethylation *in vitro*, inside Cells, and in Brain Tissues.

See also Figure S5, Table S2, and Table S3.

(A) Quantification of the m^{1}A/G ratio in total tRNA purified from HeLa, HEK293T, and 3T3-L1 cells by LC-MS/MS. The transient knockdown led to an increase of at least ~15% of the m^{1}A/G ratio in total tRNA compared to control cells.

(B) A consistent decrease (~20%) of the total tRNA m^{1}A/G ratio was observed upon overexpression of ΔNLS-FTO compared to the control.

(C) Transient knockdown of FTO led to a significant increase of both nuclear and cytoplasmic total tRNA m^{1}A/G ratio in HEK293T cells.

(D) A significant increase of m^1A in tRNA but not m^6A or m^6A_m in the polyadenylated RNA was observed in the *Fto*$^{-/-}$ MEF cells compared to the wild-type MEF cells.
(E) Knockout of *Fto* led to significant increases of both nuclear and cytoplasmic tRNA m^1A levels in tRNA in MEF cells.
(F) A significant increase of the total tRNA m^1A but not polyadenylated RNA m^6A or m^6A_m could be observed in *Fto*$^{-/-}$ mouse brain tissues compared to wild-type mouse brains.
(G) Demethylation of m^1A in tRNA isolated from HEK293T cells by recombinant FTO. EDTA chelates cofactor iron and inactivates FTO. The ratio of m^1A/G was shown. *P* values were determined using Student's unpaired t-test. *p < 0.05, **p < 0.01, ***p < 0.001, ****p < 0.0001. *n.s.* means not significant. Error bars, mean ± s.d. for $n = 4$ experiments in (A) to (E); for $n = 5$ experiments in (F); for $n = 3$ experiments in (G).

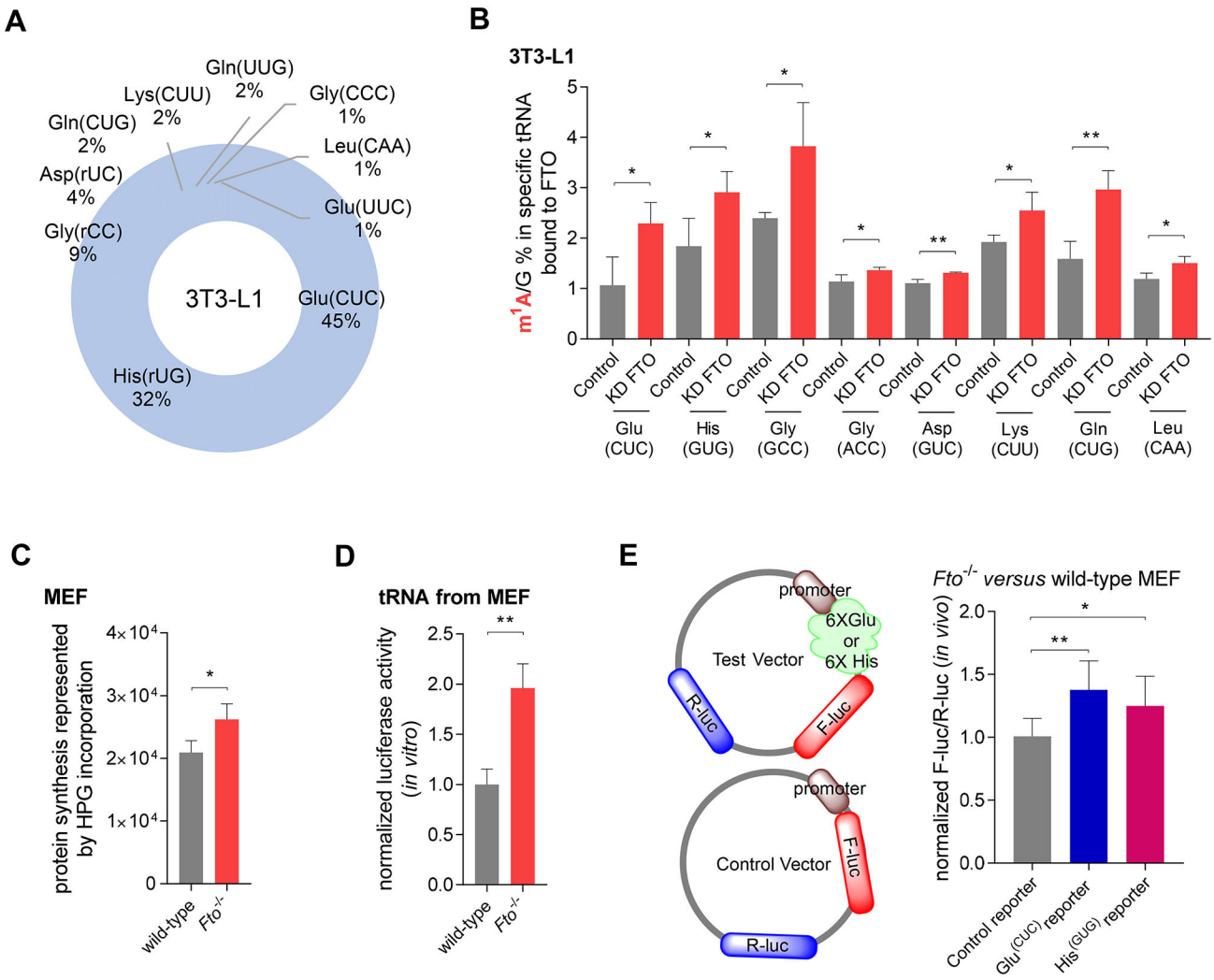

Figure 6. FTO Mediates Specific tRNA m^{1}A Demethylation and Suppresses Translation.

See also Figure S6.

(A) Pie chart showing the top FTO-bound tRNAs identified by CLIP-seq with FLAG-tagged FTO in 3T3-L1 cells.

(B) Quantification of the m^{1}A/G ratio in tRNA targets bound to FTO by LC-MS/MS. In comparison to the control, m^{1}A/G ratios of tRNA$^{Glu(CUC)}$, tRNA$^{His(GUG)}$, tRNA$^{Gly(GCC)}$, tRNA$^{Gly(ACC)}$, tRNA$^{Asp(GUC)}$, tRNA$^{Lys(CUU)}$, tRNA$^{Gln(CUG)}$, and tRNA$^{Leu(CAA)}$ noticeably increased upon transient knockdown of FTO in 3T3-L1 cell.

(C) Quantification of total protein synthesis in MEF cells by flow cytometry. HPG incorporation into wild-type MEF cell was recorded in gray and the *Fto*$^{-/-}$ MEF cells in red.

(D) Supplementation of total tRNA purified from *Fto*$^{-/-}$ MEF cell leads to increased translation efficiency *in vitro* compared to using the total tRNA from wild-type MEF cells.

(E) Cartoon illustration of the reporter assays was shown: firefly luciferase (F-luc) was used as the reporter and *Renilla* luciferase (*R*-luc) on the same plasmid was used as the internal transfection control. 6 × GUG(Glu)-coding sequences (recognized by tRNAGlu(CAC)) and 6 × CAC(His)-coding sequences (recognized by tRNAHis(GUG)) were inserted after the

PLK promoter region of F-luc as the positive reporter, respectively. The effects of $tRNA^{Glu(CUC)}$ and $tRNA^{His(GUG)}$ were revealed by the reporter assay. The reporter assay showed significant increases of protein synthesis in the *Fto*$^{-/-}$ MEF cell compared to the wild-type MEF cell when the control reporter and test reporters (with inserted Glu(CUC)-coding sequence or His(GUG)-coding sequence) are transiently expressed in the wild-type and *Fto*$^{-/-}$ MEF cell, respectively. *P* value was determined using Student's unpaired t-test. *p < 0.05, **p < 0.01, ***p < 0.001, ****p < 0.0001. *n.s.* means not significant. Error bars, mean ± s.d. for $n = 3$ experiments in (B) and (C); $n = 8$ experiments in (D) and (E).

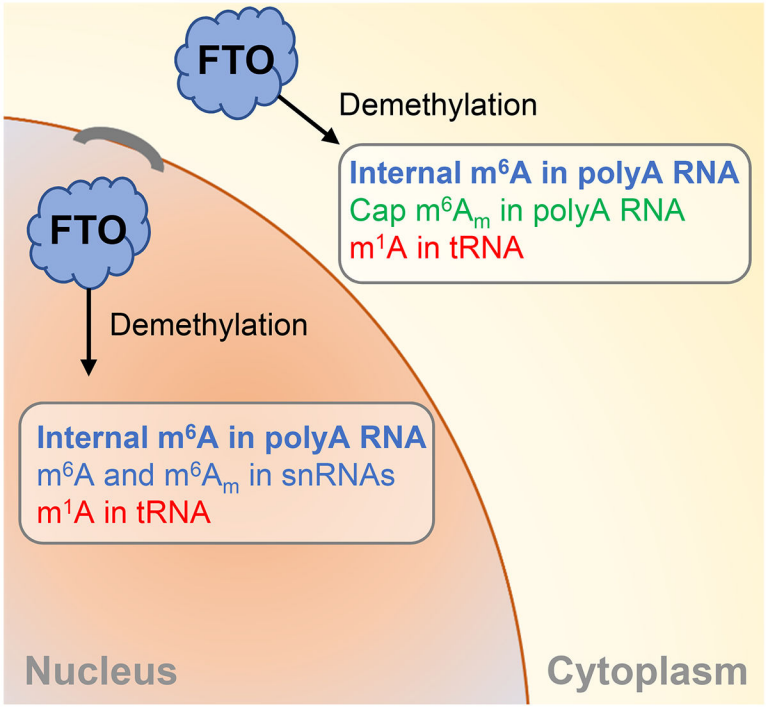

Figure 7. A Model for FTO-mediated RNA Demethylation.

Nuclear m^6A is the main substrate of FTO in the cell nucleus. FTO also mediates m^1A tRNA demethylation as well as m^6A (U6) and m^6A_m (U2 in particular but also U1) snRNA demethylation in the nucleus. FTO can localize to the cytoplasm and mediate mRNA m^6A and cap m^6A_m demethylation as well as tRNA m^1A demethylation in the cytoplasm.